International Journal of Nanomedicine

Dovepress
Taylor & Francis Group

Open Access Full Text Article

ORIGINAL RESEARCH

An Injectable Photothermal Responsive Liposome Hydrogel Co-Loaded with Bufalin, Apatinib, and IR820 for Inhibiting Postoperative Recurrence of Colon Cancer

Ai-Jia Wang[1,*], Huan Tian[2,*], Zhan-Peng Wang[1,*], Jiang-Xue Cheng[1], Jing Sun[1], Feng Zhao[2], Ya-Jun Shi[1], Xiao-Fei Zhang[1], Jun-Bo Zou[1], Fei Luan[1], Bing-Tao Zhai[1], Dong-Yan Guo[1]

[1]State Key Laboratory of Research & Development of Characteristic Qin Medicine Resources (Cultivation), and Shaanxi Province Key Laboratory of New Drugs and Chinese Medicine Foundation Research, Shaanxi University of Chinese Medicine, Xi'an, 712046, People's Republic of China; [2]Department of Pharmacy, Xi'an Hospital of Traditional Chinese Medicine, Xi'an, 710021, People's Republic of China

*These authors contributed equally to this work

Correspondence: Bing-Tao Zhai; Dong-Yan Guo, Email zbp@sntcm.edu.cn; 2051080@sntcm.edu.cn

Background: Colon cancer ranks as the third most common malignant tumor globally. Due to incomplete surgical resection and the multidrug resistance of tumor cells, it exhibits a high postoperative recurrence rate. Consequently, there is an urgent need to develop novel therapeutic strategies to inhibit postoperative recurrence of colon cancer.

Methods: Thermosensitive liposomes (Bu&Ap-Lip) co-loaded with bufalin (Bu) and apatinib (Ap) were prepared via the thin-film hydration method, with optimization of Prescription Processes. Bu&Ap-Lip was co-encapsulated with new indocyanine green (IR820) within an injectable PLGA-PEG-PLGA hydrogel, establishing a photothermally responsive composite hydrogel (Bu&Ap-Lip@IR820 Gel). The system characterized the physicochemical properties, rheological characteristics, and drug release behavior of the hydrogel, and further evaluated its in vitro antitumor activity and in vivo efficacy against postoperative recurrence of colon cancer.

Results: Bu&Ap-Lip@IR820 Gel demonstrated excellent injectability and photothermally responsive drug-release properties. In vitro cellular experiments demonstrated that Bu&Ap-Lip@IR820 Gel effectively inhibited tumor cell migration, invasion, and angiogenesis. In vivo studies revealed that this liposome hydrogel prolonged local drug retention. When combined with near-infrared light irradiation, Bu&Ap-Lip@IR820 Gel significantly suppressed tumor recurrence while exhibiting favorable in vivo biocompatibility.

Conclusion: This study developed a NIR-responsive composite liposome hydrogel integrating Bu multi-targeted antitumor properties, Ap anti-angiogenic effects, and IR820 photothermal therapeutic advantages. Through near-infrared responsiveness, it achieves localized precision drug release, effectively suppressing postoperative recurrence. This provides a novel and promising strategy for the clinical prevention and treatment of colon cancer recurrence.

Keywords: temperature-sensitive hydrogel, multimodal therapy, recurrence of colon cancer, photothermal response, drug delivery

Introduction

Globally, colon cancer ranks third in incidence and second in mortality among malignant tumors.[1] Laparoscopic surgery combined with adjuvant chemotherapy is currently the preferred clinical treatment for colon cancer.[2] However, due to incomplete surgical resection and multidrug resistance (MDR) of tumor cells, about 33% of colon cancer patients will still have tumor recurrence after treatment, and the proportion of recurrence in the first three years after surgery is more than 80%.[3,4] Although intraoperative intraperitoneal chemotherapy can effectively reduce the postoperative recurrence rate of colon cancer, the drug dose is not easy to control. Excessive local concentration and uneven distribution can easily cause nausea, vomiting, peritonitis, intestinal obstruction, and other adverse reactions, which seriously affect the quality

https://doi.org/10.2147/IJN.S575430
Received: 19 October 2025
Accepted: 2 March 2026
Published: 13 March 2026

Graphical Abstract

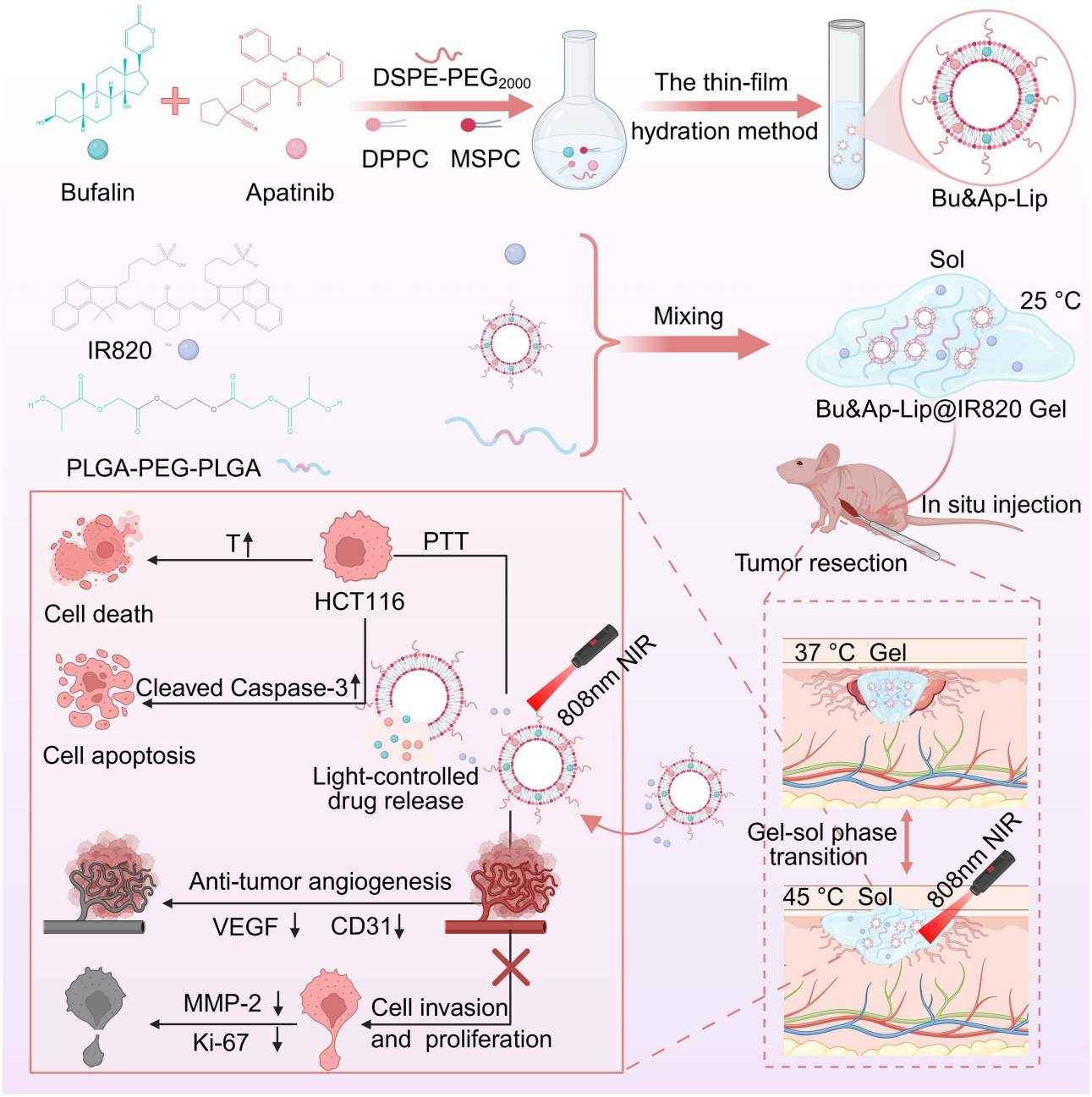

of life of patients.[5] In addition, due to the influence of individual differences, some patients cannot tolerate intraoperative chemotherapy and can only undergo subsequent systemic intravenous chemotherapy.[6] Therefore, it is important to find more effective methods to inhibit the recurrence of colon cancer after surgery.

Photothermal therapy (PTT) is considered a highly promising anti-tumor treatment strategy due to its minimally invasive, precise, controllable, and highly effective characteristics.[7–12] Indocyanine green (ICG) is a near-infrared (NIR) dye approved by the US FDA for clinical use. New indocyanine green (IR820) is an NIR dye with a structure and properties similar to ICG.[13,14] Compared to ICG, IR820 has a longer plasma half-life, higher photothermal efficiency, greater photostability, and lower photobleaching performance.[15–18] It is worth noting that IR820 has been proven to be

able to effectively inhibit the growth and recurrence of colon cancer through PTT in combination with other therapies.[19,20] Tumor angiogenesis is a key promoter of postoperative tumor recurrence, and aberrantly active vascular endothelial growth factor (VEGF) related pathways can promote new blood vessel formation, leading to tumor recurrence.[21] Apatinib (Ap) is a small-molecule tyrosine kinase inhibitor that selectively binds to and inhibits vascular endothelial growth factor receptor 2 (VEGFR2), thereby inhibiting tumor angiogenesis.[22–24] In fact, Ap can also directly inhibit tumor cell proliferation, induce apoptosis, and reverse multidrug resistance.[25,26] Clinical studies further confirm that Ap demonstrates favorable efficacy in the treatment of colorectal cancer and significantly improves patients' quality of life.[27,28] When combined with Camrelizumab, 5-Fluorouracil, or the FOLFIRI chemotherapy regimen, can further enhance the therapeutic effect of colon cancer.[29–31] Bufalin (Bu) is an active ingredient extracted from dried toad skin in traditional Chinese medicine, and also serves as a key active ingredient in Cinobufacini capsules, a commonly used postoperative treatment for colon cancer patients.[32] Research indicates that Bu not only directly inhibits colon cancer through multiple pathways inducing apoptosis, causing cell cycle arrest, and suppressing invasion and migration but also downregulates signaling pathways such as STAT3 and PI3K/AKT/mTOR to reduce the production of pro-angiogenic factors like VEGF.[33–36] Therefore, the combined antitumor effects of Ap and Bu may involve multi-level synergistic interactions. In summary, Bu, Ap, and IR820 have significant application value in the postoperative treatment of colon cancer, but monotherapy remains limited and ineffective. Therefore, this study proposes a novel triple therapy combining traditional Chinese medicine active components with multi-targeted antitumor effects, anti-tumor angiogenesis, and PTT, effectively inhibiting postoperative recurrence of colon cancer. However, Bu has poor water solubility and strong cardiotoxicity, Ap has poor water solubility and low oral bioavailability,[37] and IR820 has limited tumor targeting ability. These factors severely restrict the clinical application of Bu, Ap, and IR820. Therefore, there is an urgent need to develop a novel system to achieve the combined delivery of the three drugs and efficiently inhibit the postoperative recurrence of colon cancer.

To achieve the synergistic effects of the three drugs, it is crucial to deliver the drugs precisely to the tumor site and ensure sustained therapeutic effects. Injectable thermosensitive hydrogels have demonstrated unique advantages in the field of local drug delivery due to their in situ gelation properties and ability to conform to irregular wound surfaces adaptively.[38,39] However, there are still several issues, such as insufficient drug synergistic effects and irregular drug release, that cannot meet the dynamic demands of the tumor microenvironment.[40] Embedding liposomes in hydrogels not only enhances the drug-carrying capacity of hydrogels but also reduces toxicity and improves drug release.[41,42] Thermosensitive liposomes (TSLs) undergo a phase transition from a gel-crystalline state to a liquid crystal state at a specific temperature, causing the phospholipid bilayer structure to become loosened, thereby enhancing membrane fluidity and permeability, and enabling controlled drug release.[43] PLGA-PEG-PLGA is a thermosensitive triblock hydrogel material that forms micelles with hydrophobic PLGA as the core and hydrophilic PEG as the crown at low temperatures.[44] Upon heating, the PEG chains dehydrate and collapse to form a hydrophobic crosslinked network, enabling a reversible "sol-gel" transition. Notably, PLGA-PEG-PLGA with specific ratios can also undergo a "gel-sol" transition at higher temperatures, but current research in this area is limited.[45] This could potentially represent a breakthrough for controlled drug release.

In summary, combining the advantages of triple therapy, TSLs, and injectable thermosensitive hydrogels, it is necessary to develop a multifunctional composite hydrogel for the prevention of postoperative recurrence of colon cancer. Therefore, in this study, Bu and Ap were first co-loaded onto TSLs to enhance the bioavailability of both drugs and reduce the cardiac toxicity of Bu. Subsequently, leveraging the high photothermal conversion efficiency of IR820 and the unique "sol-gel-sol" transformation characteristics of PLGA-PEG-PLGA, the drug-loaded TSLs and IR820 were encapsulated within the injectable hydrogel, successfully constructing a photothermal-responsive liposome-based injectable hydrogel (Bu&Ap-Lip@IR820 Gel) for postoperative local treatment. Bu&Ap-Lip@IR820 Gel can precisely deliver high concentrations of Bu, Ap, and IR820 to the treatment site, enabling controlled photothermal-responsive drug release. This ensures an optimal "effective" drug concentration at the tumor site while minimizing toxic side effects. In summary, this triple therapy based on a local hydrogel delivery system holds promise as a tool that could provide a basis for a drug delivery platform aimed at clinically inhibiting the recurrence of colon cancer post-surgery.

Materials and Methods

Materials

DPPC (C159364505, purity>99%) and IR820 (C15811515, purity>80%) were purchased from Shanghai Macklin Biochemical Co., Ltd; MSPC (CG1057, purity>99%) was purchased from AVT (Shanghai) Pharmaceutical Tech Co., Ltd.; DSPE-PEG_{2000} (ML290001, purity>98%), PLGA-PEG-PLGA thermosensitive hydrogel (ML182320) were purchased from MeloPEG Co., Ltd; Bufalin (HS21305B1, purity>98%) was purchased from Baoji Chenguang Biological Technology Co., Ltd.; Apatinib (S524804, purity>98%) was purchased from Selleckchem Chemicals.; Calcein/PI cell activity and cytotoxicity detection kit (101223240515), DiD fluorescent dye (C1039), TUNEL kit (C1088), DAPI (C1005) were purchased from Shanghai Beyotime Biotechnology Co., Ltd.; Apoptosis detection kit (AB-2869082) was purchased from Bedi Medical Device Co., Ltd.; Ki-67 (ab15580) was purchased from Abcam; Cleaved Caspase-3 (#9662) was purchased from CST; CD31 (11265-1-AP, VEGF (81323-2-RR) and MMP-2 (10373-2-AP) was purchased from Proteintech; β-actin (66009-1-Ig) was purchased from Proteintech; D-fluorescein sodium salt (D4422160) was purchased from Yeasen Biotechnology (Shanghai) Co, Ltd.; Isoflurane (2024100301) was purchased from Shandong Ante Animal Husbandry Co., Ltd.; LC-2023C 3D PLUS Shimadzu high performance liquid chromatograph (SHIMADZU, Japan); GS-1580R refrigerated centrifuge (Gene Company Limited); Ts2-FL fluorescence inverted fluorescence microscope (Nikon Technology Co., Ltd).; TD4C centrifuge (Jiangsu Datang Medical Device Co., Ltd).; 51119670DP Microplate Reader (Simmel Fisher Technology Co., Ltd).; JEM-1400FLASH transmission electron microscope (JEOL); ZS90 Malvern particle size potentiometer (Malvern Instrument Co., Ltd., UK); TESCAN VEGE3 scanning electron microscope (TESCAN Co., Ltd.); HaakeMars III Rheometer (Thermo Fisher Scientific Technology Co., Ltd.); FLUKE infrared thermal imager (Fotric Inc. Co., Ltd).; lR-MFJ-808/5000mW laser (Changchun Laser Technology Co., Ltd).; Tanon 4600 ultra-high sensitivity chemiluminescence imaging system (Shanghai Tianneng Technology Co., Ltd.); IVScope 8200 small animal living imager (Clinx Science Instruments Co., Ltd).

HCT116 cells (CL-0096) were provided by Procell Life Science & Technology Co., Ltd., and were cultured in a 5% CO_2 cell incubator at 37 °C using HCT116 cell-specific medium. NCM460 cells (ZQ1079) were provided by Shanghai Zhong Qiao Xin Zhou Biotechnology Co., Ltd., and cultured in a 5% CO_2 cell incubator at 37 °C using NCM460 cell-specific medium. HUVEC cells (IM-H205) were provided by Xiamen Immocell Biotechnology Co., Ltd, and were cultured in a special medium for HUVEC cells at 37 °C and 5% CO_2 cell incubator. HCT116-Luc cells (TCH-C185L) were provided by Suzhou Starfish Biotechnology Co., Ltd. HCT116-Luc cells were cultured in a 5% CO_2 incubator at 37°C.

BALB/c nude mice, SPF grade, female, 4–6 weeks old, weighing 20 ± 2 g, purchased from Chengdu Dashuo Experimental Animal Co., Ltd. (Chengdu, China, licensed ID: SCXK (Chuan) 2020–0030). Feeding environment: room temperature 25 °C, relative humidity 50% ~ 60%, circadian rhythm light, giving nude mice free drinking water and food. All animal experiments were approved by the Experimental Animal Welfare and Ethics Management Committee of Shaanxi University of Traditional Chinese Medicine (Ethical batch number: SUCMDL20240821004). Additionally, this study was conducted in accordance with the National Institutes of Health guidelines for the use of experimental animals.

Determination of Bu and Ap

A method for the simultaneous determination of Bu and Ap was established by high-performance liquid chromatography (HPLC). Chromatographic column: HyPURITY C18 chromatographic column (250 mm × 4.6 mm, 5 μm); Mobile phase: acetonitrile/0.3% phosphoric acid aqueous solution (40:60, v/v); Flow rate: 1.0 $mL \cdot min^{-1}$; Column temperature: 30 °C; Detection wavelength: 260 nm (Ap), 296 nm (Bu); Injection volume: 10 μL. The specificity, detection limit, quantitative limit, linear relationship, precision, stability, repeatability and recovery rate were investigated.

Preparation and Characterization of Bu&Ap-Lip

Screening of Bu/Ap Synergistic Ratio

MTT assay was used to detect the toxicity of Bu and Ap alone and in combination with different proportions on HCT116 colon cancer cells. The cells were inoculated in a 96-well cell culture plate at 1.0×10^4 cells/well and incubated at 37 °C

for 12 h. Each group was treated for 24 h. The culture plate was taken out, and 20 μL MTT was added to each well. After 4 h of incubation, 150 μL of dimethyl sulfoxide was added and transferred to a microplate reader to determine the absorbance (A) value at 490 nm in each group, and the cell survival rate was calculated. Based on the IC_{50} value of Bu and Ap, the combination index (CI) was calculated by CompuSyn software based on the Chou-Talalay combination theory, and the toxic effect of Bu and Ap on HCT116 cells was analyzed.

Preparation Process of Bu&Ap-Lip

Bu&Ap-Lip was prepared by the thin film dispersion method. According to the mass ratio of 25: 2: 3: 0.003: 1.5, DPPC, MSPC, DSPE-PEG_{2000}, Bu and Ap were accurately weighed and mixed in an eggplant-shaped flask, and then 1 mL of anhydrous methanol solution was added. After ultrasonic dissolution, it was evaporated under reduced pressure at 40 °C and 100 rpm until a transparent and uniform lipid film was formed on the inner wall. Subsequently, 1 mL of preheated PBS at 60 °C was added, and the mixture was rotated and hydrated at 60 °C and 120 rpm for 50 min. After ultrasonic treatment and transmembrane, Bu&Ap-Lip was obtained and sealed at 4 °C for further use. The preparation steps of blank liposomes (Lip) are the same as Bu&Ap-Lip, except that Bu and Ap are not contained.

Designs of Single Factor Experiments of Bu&Ap-Lip

The encapsulation efficiency (EE) of Bu and Ap was used as an evaluation index to optimize the preparation process of Bu&Ap-Lip. The effects of different membrane material ratios (DPPC: MSPC), DSPE-PEG_{2000} addition amount, ratio of drug to lipid, rotary evaporation temperature, hydration temperature, and hydration time on the encapsulation efficiency of Bu and Ap in Bu&Ap-Lip were investigated by single factor experiment.

Optimization of the Prescription Process of Bu&Ap-Lip by Response Surface Methodology

Based on the results of single factor investigation, the %EE (Y) of Bu and Ap in liposomes was used as the response value, and the three variables of membrane material ratio (A), DSPE-PEG_{2000} addition amount (B) and ratio of drug to lipid (C) were selected as the experimental factors. Design-Expert 13.0 software was used to design these three factors at three levels. The EE of Bu and Ap in Bu&Ap-Lip was used as the evaluation index to optimize the preparation process of Bu&Ap-Lip further. Subsequently, three batches of drug-loaded liposomes were prepared by the selected optimal process, and the reliability of the process was verified by measuring the EE of Bu and Ap in liposomes.

Particle Size Distribution and Zeta Potential of Bu&Ap-Lip

Bu&Ap-Lip was stained with 2% phosphotungstic acid solution for 1 min, and the micromorphology of liposomes was observed by transmission electron microscopy (TEM). The changes of particle size, Zeta potential and PDI of liposomes without heating or after heating at 50 °C were determined by dynamic light scattering (DLS) using a Malvern particle size potentiometer.

Determination of EE and Drug Loading of Bu and Ap in Bu&Ap-Lip

An appropriate amount of Bu&Ap-Lip was taken, and the drug-loaded liposomes and free drugs were separated by ultrafiltration centrifugation (10 kDa). The contents of Bu and Ap in liposomes were determined by HPLC, and the EE and drug loading (DL) of the two drugs in liposomes were calculated.

$$EE(\%) = \frac{W_e}{W_t} 100\%$$

$$DL(\%) = \frac{W_e}{W_l} 100\%$$

Among them, W_t: Total mass of liposome drug, W_e: Quality of liposome encapsulated drugs, W_l: Total mass of liposomes

https://doi.org/10.2147/IJN.S575430

Stability Study

The prepared liposomes were stored in the dark at 4 °C and 25 °C for 14 days, respectively. The particle size and PDI of liposomes were measured every 2 days to investigate the stability of the prepared drug-loaded liposome solution at different temperatures.

Fluorescence Quenching Method for Measuring Temperature-Sensitive Release from Liposomes

Using the method described in Preparation Process of Bu&Ap-Lip, Ca-loaded liposomes (Ca-Lip) were prepared with Calcein (Ca) aqueous solution as the hydration medium. Unencapsulated free Ca was removed via ultrafiltration centrifugation. Precisely pipette 1 mL of Ca-Lip into 50 mL of PBS and magnetically stir at different temperatures. Samples of 200 μL were taken at 0 and 30 min, diluted to 2 mL with PBS, and fluorescence values were measured. Magnetic stirring was performed at 45 °C. Samples were taken at 1, 5, 10, 20, 40, 60, and 120 min for measurement, and the cumulative release rate of Ca was calculated.

$$\text{Calcein release}\,(\%) = \frac{(I_t - I_0)}{(I_\infty - I_0)}\,100$$

Among them, I_0: Initial fluorescence value, I_t: Fluorescence values at different times, I_∞: Fluorescence intensity of liposomes treated with Triton X-100

Preparation and Characterization of Bu&Ap-Lip Gel

Preparation of Bu&Ap-Lip@IR820 Gel

Precisely weigh 0.875 g of PLGA-PEG-PLGA into a test tube, add 5 mL of Bu&Ap-Lip solution, and allow it to swell fully at 25 °C for 48 hours. After swelling, precisely add an appropriate amount of IR820 (1 mg) and stir thoroughly to obtain the Bu&Ap-Lip@IR820 gel precursor solution. Store it at 4 °C in the dark for later use. The preparation steps for the blank hydrogel (Gel), blank liposome loaded hydrogel (Lip Gel), Bu&Ap-Lip loaded hydrogel (Bu&Ap-Lip Gel), IR820 loaded hydrogel (IR820 Gel) and blank liposome and IR820-loaded hydrogel (Lip@IR820 Gel) are the same as those for Bu&Ap-Lip@IR820 Gel.

Phase Diagram of Bu&Ap-Lip@IR820 Gel

In this experiment, PLGA-PEG-PLGA was selected as the matrix material of thermosensitive hydrogel, and the optimal concentration was screened by phase transition temperature. Bu&Ap-Lip@IR820 Gel with concentrations of 10.0%, 12.5%, 15.0%, 17.5% and 20.0% were prepared in turn. The "sol-gel-sol" phase transition temperature in the range of 25 ~ 55 °C was determined by the flip method. Plot temperature-phase transition curves using software. Establish phase diagrams to reveal quantitative relationships between copolymer concentration, temperature, and phase states.

Photothermal Conversion Properties of Bu&Ap-Lip@IR820 Gel

Place 1 mL of Bu&Ap-Lip@IR820 Gel containing different concentrations of IR820 into 2 mL centrifuge tubes. Position the tubes in a 37°C water bath until a semi-solid hydrogel forms. Irradiate with an 808 nm (2.5 $W{\cdot}cm^{-2}$) NIR laser for 5 minutes. The gel temperature was recorded every 0.5 minutes using a FLUKE infrared thermal imaging camera. 1 mL of Bu&Ap-Lip@IR820 Gel containing different IR820 concentrations was placed in a quartz cuvette and irradiated with an 808 nm (2.5 $W{\cdot}cm^{-2}$) laser for 1 minute, with temperature readings taken every 0.1 minute. Following 1 minute of irradiation, the laser was switched off. Upon cooling to 37 °C, irradiation was repeated for 1 minute under identical conditions. This "ON" and "OFF" cycle was repeated five times, with gel temperature recorded using the FLUKE infrared thermal imager.

Appearance Character and Preliminary Stability Investigation

Gel and Bu&Ap-Lip@IR820 Gel were placed at room temperature, 37 °C and 50 °C for 15 min, respectively, to observe the state changes of Gel and Bu&Ap-Lip@IR820 Gel. In addition, 1 mL of Bu&Ap-Lip@IR820 Gel was precisely sucked into a glass bottle, and 3 mL of purified water, saline, PBS, complete medium, and fetal bovine serum were added, respectively. After vortex mixing, each sample was placed at room temperature in the dark for 7 days to observe its state changes.

Investigation of Microstructure and Injectability

The cross-sectional morphology of Bu&Ap-Lip@IR820 Gel was observed by scanning electron microscopy (SEM). The plastic petri dish was placed in a thermostatic water bath at 37 °C, and the Gel and Bu&Ap-Lip@IR820 Gel precursor solutions were written in a plastic petri dish using a 1 mL needle syringe to write the letter "ABC" or injected into pure water at 37 °C to investigate the injectability of the hydrogel.

Swelling Performance Investigation

After the hydrogel is implanted in the body, the swelling stress may have adverse effects on the surrounding tissues. Therefore, the swelling properties of Bu&Ap-Lip@IR820 Gel were investigated by the gravimetric method. 1 mL of Gel, Bu&Ap-Lip Gel, Bu&Ap-Lip@IR820 Gel was placed in a test tube, and 10 times the amount of water was added. After 24 h, the water in the test tube was discarded, weighed and recorded.

Investigation of Rheological Properties

The rheological properties of Gel and Bu&Ap-Lip@IR820 Gel were tested by a HaakeMars III rheometer. The temperature scanning experiment with the temperature range from 25 °C to 55 °C and the heating rate of 2 $°C \cdot min^{-1}$ was carried out under the condition of 1% constant strain and 1 Hz constant frequency. The isothermal time scanning experiment of 60 s was carried out at a constant temperature of 37 °C, a constant frequency of 1 Hz and a constant strain of 1%. Under the condition of 37 °C constant temperature and 1% constant strain, the frequency scanning experiment with a frequency range from 200 $rad \cdot s^{-1}$ to 0.1 $rad \cdot s^{-1}$ was carried out. Under the condition of constant temperature of 37 °C and constant frequency of 1 Hz, the strain scanning experiment with a strain range from 0.01% to 100% was carried out. At a constant temperature of 37 °C and a constant frequency of 1 Hz, a large strain (500%) was applied in the first 120 s, and then a small strain (1%) was applied. The cyclic strain scanning experiment was repeated five times.

Investigation of Photothermal Properties

1 mL of pure water, Bu&Ap-Lip Gel, IR820 Gel and Bu&Ap-Lip@IR820 Gel were gelatinized at 37 °C, and then irradiated with 808 nm laser (2.5 $W \cdot cm^{-2}$) for 5 min. The FLUKE infrared thermal imager was used to collect images every 0.5 min and record the temperature of the hydrogel and draw the heating curve. Bu&Ap-Lip@IR820 Gel was subjected to 5 laser "ON/OFF" cycles (1 min irradiation/cooling to 37 °C). The temperature was recorded every 0.1 min and the cycle curve was drawn to test its photothermal stability.

In vitro Drug Release Studies

The drug release characteristics of Bu&Ap-Lip@IR820 Gel under near-infrared light (808 nm) irradiation were investigated. They were divided into two groups: I. Bu&Ap-Lip@IR820 Gel group, II. Bu&Ap-Lip@IR820 Gel + L group. At room temperature, 1 mL of Bu&Ap-Lip@IR820 Gel precursor solution was injected into a 5 mL brown glass bottle and then placed in a 37 °C water bath. After the gel was formed, 1 mL of 37 °C release medium (PBS containing 0.5% Tween80) was injected, and slowly shaken in a 37 °C water bath shaker. Group II at 1 and 2 h., the 808 nm laser (2.5 $W \cdot cm^{-2}$) was used to irradiate for 1 min, and all the release media of the two groups were absorbed at the preset time (0, 0.5, 1, 2, 4, 6, 8, 10, 12, 24 h, 36 h, 48 h). At the same time, 1 mL of isothermal and an equal amount of fresh release medium were immediately added. The collected release medium was diluted and filtered, and the Ap content was determined by HPLC.

Anti-Tumor Effect of Bu&Ap-Lip@IR820 Gel in vitro

In vitro Biocompatibility

MTT assay was used to detect the toxicity of Gel and Lip@IR820 Gel to NCM460 cells. After the hydrogel was solidified at 37 °C, it was extracted with medium for 24 h, filtered and diluted to different concentrations (0%, 25%, 50%, 75%, 100%). NCM460 cells were inoculated in 96-well plates at a density of 1.0×10^4 cells/well. After incubation for 12 h, different concentrations of hydrogel extract were added, and the survival rate was detected after incubation for 24 h. In vitro hemolysis test was used to evaluate blood compatibility: 5% red blood cell suspension was incubated with

different concentrations of hydrogel extract at 37 °C for 4 h, and the absorbance at 545 nm was measured after centrifugation. The hemolysis rate was calculated with water (positive) and PBS (negative) controls.

In vitro Cytotoxicity

The cytotoxic effects of different drugs on HCT116 cells were determined by MTT assay. The cells were seeded in 96-well plates at a density of 1.0×10^4 cells/well and incubated for 12 h. Add 100 μL drug-containing culture: I. Control, II. L, III. Lip Gel, IV. Lip@IR820 Gel + L, V. Bu&Ap-Lip@IR820 Gel, VI. Bu&Ap-Lip@IR820 Gel + L. In groups II, IV and VI, the hydrogel area was irradiated with 808 nm NIR laser (2.5 $W\cdot cm^{-2}$) for 5 min, and then incubated for 24 h. After that, 20 μL of MTT solution was added. After incubation for 4 h, the medium was removed and 150 μL dimethyl sulfoxide was added to each well. The absorbance of each well was measured using a microplate reader at 490 nm, and the cell survival rate was calculated.

In vitro Photothermal Effect

Based on colon cancer HCT116 cells, the in vitro photothermal effect of Lip@IR820 Gel on HCT116 cells was further evaluated by live-dead cell staining assay. The experiment was divided into 6 groups: I. Control, II. L, III. Lip Gel + L, IV. IR820 + L, V. Lip@IR820 Gel, VI. Lip@IR820 Gel + L. HCT116 cells were seeded into 24-well plates at a density of 1.0×10^5 cells/well and incubated for 12 h. The hydrogel was injected into the Transwell chamber, and the chamber was placed in a 24-well plate after being transformed into a gel state at 37 °C. After 10 min, the hydrogel area of groups II, III, IV and VI was irradiated with 808 nm NIR laser (2.5 $W\cdot cm^{-2}$) for 5 min. Then Calcein/PI cell activity and cytotoxicity detection kit was used for staining and examined under a fluorescence microscope. To further quantify the cell death induced by the photothermal temperature increase, cell apoptosis was analyzed by flow cytometry.

Cell Apoptosis Assay

The pro-apoptotic properties of Bu&Ap-Lip@IR820 Gel were investigated by flow cytometry. HCT116 cells were seeded in 6-well plates at a density of 5.0×10^5 cells/well and incubated for 12 h. The experimental groups were the same as in vitro cytotoxicity assay, and the apoptosis was detected by flow cytometry and analyzed systematically according to the instructions of the apoptosis detection kit.

Cell Migration Assay

HCT116 cells were seeded in a 6-well plate at a density of 1.5×10^6 cells/well and incubated in a cell incubator. When the cell fusion degree reached 90%, the cell layer was quickly lightly scratched with a 10 μL sterile gun. The scratch width was observed and recorded under an inverted microscope, and the time point was recorded as 0 h. The experimental groups were the same as in vitro cytotoxicity assay. The scratches of each group were photographed and recorded using an inverted microscope, and the scratch area was statistically analyzed by ImageJ 1.52.

Cell Invasion Assay

The Matrigel was diluted with serum-free medium, and 60 μL/well was added to the Transwell upper chamber, incubated at 37 °C for 1 h to solidify, and then 100 μL of serum-free medium was added for hydration for 30 min. HCT116 cells cultured in serum-free medium for 24 h were adjusted to a density of 1.5×10^5 cells/mL, and 100 μL of cell suspension was inoculated into the upper chamber of the Transwell. The experimental groups were the same as in vitro cytotoxicity assay, and 1 mL of hydrogel extract was added to the lower chamber. After 24 h of culture, the upper chamber medium was removed, stained with 0.1% crystal violet for 30 min, and randomly observed under a microscope after drying. The transmembrane cells were quantitatively analyzed by ImageJ 1.52.

Tube Formation Assay

The Matrigel was diluted with pre-cooled DMEM basal medium. 50 μL of matrix gel diluent was added to each well of the 96-well plate, and then the 96-well plate was incubated in an incubator at 37 °C for 1 h to coagulate; the density of HUVEC cells was adjusted to 6×10^5 cells/mL, and 50 μL per well was inoculated in 96-well plates. The experimental groups were the same as in vitro cytotoxicity assay, and incubated for 4 h after administration. The field of view was

selected using an inverted microscope, observed and recorded. Finally, the ImageJ plug-in Angiogenesis Analyzer was used for quantitative analysis.

Western Blot

The drug-treated HCT116 cells were washed with PBS and extracted with 100 μL pre-cooled protein lysis buffer (RIP). GAPDH was used as the internal reference protein. After protein separation in 10% SDS-PAGE gel electrophoresis, it was transferred to a PVDF membrane. The sample was blocked and incubated with Ki-67, Cleaved Caspase-3, MMP-2, VEGF and CD31 at 4 °C overnight. The secondary antibody was added and incubated on a shaker at room temperature for 2 h. After incubation, the developer was added at room temperature, incubated in the dark for 3 min, exposed, and visualized on a super-sensitive chemiluminescence imaging system. The gray value of protein bands was statistically analyzed by Image J 1.52, and the difference in protein expression between groups was compared.

In vivo Animal Experiments

In vivo Biocompatibility and Retention

The Bu&Ap-Lip@IR820 Gel precursor solution was implanted subcutaneously into the back of BALB/c nude mice. The general condition and mortality of mice were observed. The tissues around the injection site were carefully removed at the predetermined time, and histopathological examination was performed by HE staining.

The IVIS in vivo imaging system was used to investigate the in vivo retention of Bu&Ap-Lip@IR820 Gel after implantation in nude mice. The hydrophobic fluorescent dye DiD was selected to replace Bu and Ap to prepare a drug-loaded liposome hydrogel (DiD-Lip@IR820 Gel) for in vivo experiments. BALB/c nude mice were randomly divided into three groups: I. DiD (DiD: 1.5 $mg{\cdot}mL^{-1}$, 100 μL), II. DiD-Lip@IR820 Gel (IR820: 0.2 $mg{\cdot}mL^{-1}$), III. DiD-Lip@IR820 Gel + L. Group III was irradiated with 808 nm laser (2.5 $W{\cdot}cm^{-2}$) for 1 min on the 1 st and 2 nd day after implantation. At the specified time points, DiD fluorescence images were obtained using the IVIS in vivo imaging system with excitation and emission wavelengths of 646 and 663 nm, and fluorescence intensity quantitative analysis.

In vivo Photothermal Effect

Based on the subcutaneous colon cancer resection model of BALB/c nude mice, the temperature rise of Bu&Ap-Lip@IR820 Gel hydrogel injection site under NIR laser irradiation was investigated. The experiment was divided into 4 groups: I. Saline group (100 μL), II. Lip Gel, III. Lip@IR820 Gel, IV. Bu&Ap-Lip@IR820 Gel. The samples were injected into the tumor resection site of BALB/c nude mice after the operation. Each group was irradiated with an 808 nm (2.5 $W{\cdot}cm^{-2}$) NIR laser for 5 min. The images were collected by a FLUKE infrared thermal imager and the temperature of the sample implantation site was recorded every 0.5 min.

In vivo Anti-Tumor Recurrence Effect

100 μL HCT116-Luc cells were inoculated into the right axilla of BALB/c nude mice at a concentration of $2{\times}10^7$ cells/mL and fed normally. After 7 days of inoculation, when the tumor volume reached about 100 mm^3, the nude mice were anesthetized with isoflurane. About 95% of the visible tumor tissue was removed under sterile conditions, and 5% of the tumor tissue was intentionally left around the operating table to simulate the real postoperative tumor tissue cell residue. The nude mice were randomly divided into 6 groups: I. Saline (100 μL); II. Bu + Ap (Bu: 0.003 $mg{\cdot}mL^{-1}$, Ap: 1.5 $mg{\cdot}mL^{-1}$); III. Lip Gel group; IV. Lip@IR820 Gel + L group (IR820: 0.2 $mg{\cdot}mL^{-1}$); V. Bu&Ap-Lip@IR820 Gel group; VI. Bu&Ap-Lip@IR820 Gel + L group. The drug was directly injected into the residual tumor site to form a gel, and the wound was closed and disinfected with 6.0 silk thread. Groups IV and VI were irradiated with 808 nm NIR laser (5 min each time, the power density was manually adjusted to 45 °C) after 1 d and 2 d of administration. The body weight of each mouse was measured and recorded every 2 days, and the body weight-time curve was drawn. IVIS bioluminescence imaging was used to monitor tumor recurrence once a week under isoflurane anesthesia. The recurrence rate and mortality rate of mice were counted. The time of local recurrence was defined as the subcutaneous nodules with obvious protrusions detected at the surgical site on the same day. At the end of the experiment, all the resected tumors were photographed and weighed, and the tumor recurrence inhibition rate was calculated. The anti-tumor recurrence experiment was continuously monitored for 28 days. After anesthesia with isoflurane inhalation, the mice were humanely

sacrificed, and then the tumor tissue and the main organs such as heart, liver, spleen, lung and kidney were dissected, and fixed with 4% paraformaldehyde for HE staining. Tumor tissues were subjected to TUNEL staining, Ki-67, Cleaved Caspase-3, MMP-2 and VEGF immunohistochemical staining, and CD31 immunofluorescence staining. In addition, blood routine tests and serum biochemical index tests were carried out to verify the biosafety of the hydrogel.

Statistical Analysis

SPSS 26.0 software was used to analyze the data. Visualization is performed by GraphPad Prism 9.0. The results were expressed as mean ± standard deviation (Mean ± SD). The *t*-test was used to analyze the differences between the two groups. One-way analysis of variance (ANOVA) was used to evaluate the differences between multiple groups, and Tukey's test was used for post-hoc comparisons. A $p < 0.05$ was considered statistically significant.

Results

The Establishment of the Bu and Ap Content Analysis Method

Bu and Ap were well separated at 296 nm and 260 nm, respectively, indicating that the chromatographic conditions were suitable for the separation of Bu and Ap. The standard curve equation of Bu was Y = 18572X + 377.24, $R^2 = 0.9997$, the linear range was 0.20 ~ 25 μg·mL^{-1}, the limit of quantitation and the limit of detection were 0.2541 μg·mL^{-1} and 0.0762 μg·mL^{-1}, respectively. The precision, stability, repeatability and sample recovery of this method were good, and the RSD values were 1.02%, 0.93%, 1.11% and 1.49%, respectively. The standard curve equation of Ap was Y = 60143X + 22919, $R^2 = 0.9999$, the linear range was 0.49 ~ 62.5 μg·mL^{-1}, the limit of quantitation and the limit of detection were 0.0517 μg·mL^{-1} and 0.0155 μg·mL^{-1}, respectively. The precision, repeatability, stability and sample recovery of this method were good, and the RSD values were 0.74%, 0.84%, 0.66% and 1.03%, respectively. The detailed information is shown in supplementary materials (Figures S1, S2 and Tables S1–S4).

Preparation and Characterization of Bu&Ap-Lip

First, the IC_{50} values of Bu and Ap when used alone on HCT116 cells for 24 hours were determined using the MTT assay, yielding values of 22.87 ± 0.68 ng·mL^{-1} and 14.72 ± 0.44 μg·mL^{-1}, respectively (Figure 1A and B). Subsequently, using CompuSyn software, when Bu and Ap were used in combination at a mass ratio (ng/μg) of 2:1, the CI value was minimal (Figure 1C and D), indicating the strongest synergistic effect between the drugs,[46] providing preliminary pharmacodynamic evidence for subsequent formulation preparation. DPPC is a commonly used material for preparing TSLs. Adding MSPC during the preparation process not only enables TSLs to obtain more stable drug release pores in a fluid state but also lowers the phase transition temperature of TSLs, thereby reducing high-temperature damage to normal tissues.[47] Adding DSPE-PEG_{2000} can extend the circulation time in the body.[48] Therefore, this study selected DPPC, MSPC, and DSPE-PEG_{2000} as membrane materials and used the thin-film dispersion method to prepare TSLs encapsulating Bu and Ap (Bu&Ap-Lip). Through single-factor experiments combined with Box-Behnken optimization, the optimal formulation and process for Bu&Ap-Lip were determined, with the final parameters adjusted to a membrane material ratio of 12.5:1, the DSPE-PEG_{2000} addition amount was 3 mg, and the drug-to-lipid ratio was 1:20 (Figure S3 and Tables S5–S7). The Bu&Ap-Lip appeared round or oval under TEM, with smooth and flat surfaces and good dispersion (Figure 1E). The EE of Bu and Ap was 84.76 ± 2.51% and 85.43 ± 0.33%, respectively, and the DL was 0.0086 ± 0.00025% and 4.27 ± 0.02%, respectively. Liposome stability is a critical factor to consider in drug delivery systems. The stability of Bu&Ap-Lip under light-protected storage conditions at 4°C and 25°C was evaluated using particle size and PDI as indicators. It was found that the particle size and PDI of Bu&Ap-Lip showed no significant changes, indicating good stability (Figure 1F). The average particle size of Bu&Ap-Lip was 151.1 ± 1.380 nm, PDI was 0.152 ± 0.005, and Zeta potential was −17.9 ± 0.058 mV. After heating at 50°C, the average particle size of Bu&Ap-Lip changed to 228.7 ± 0.954 nm, the PDI changed to 0.350 ± 0.012, and the Zeta potential changed to −6.7 ± 0.264 mV (Figure 1G), indicating that an increase in temperature causes Bu&Ap-Lip to rupture. The results of the fluorescence quenching experiment showed that as the temperature increased, the release amount gradually increased. There was almost no release at 37 ~ 40 °C. At 41 °C, there was a sudden large amount of release (Figure S4). Therefore, 41 °C is

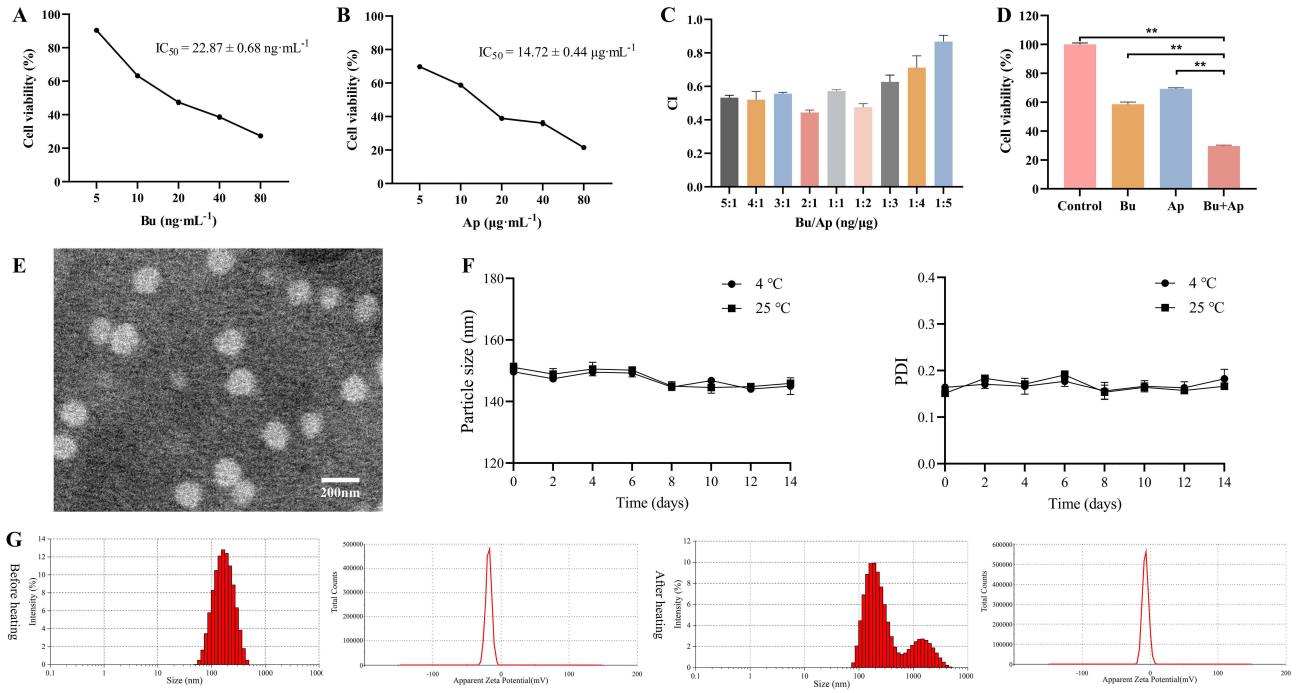

Figure 1 Characterization of Bu&Ap-Lip. (**A**) Cell viability of Bu on HCT116 cells. (**B**) Cell viability of Ap on HCT116 cells. (**C**) The combination index (CI) of different proportions of Bu and Ap. (**D**) Verification of synergistic effects of Bu and Ap. (**E**) The micromorphology of Bu&Ap-Lip. (**F**) The changes in particle size and PDI of Bu&Ap-Lip at different temperatures for two weeks. (**G**) Particle size distribution and Zeta potential distribution of Bu&Ap-Lip before and after heating. (n = 3, $^{**}p < 0.01$).
Abbreviation: CI, combination index.

approximately the phase transition temperature of Ca-Lip. Ca-Lip can achieve complete release at 45 °C, and the release speed is very fast, with 80% release within 120 min. In addition, the IC_{50} values of the drugs encapsulated in liposomes for HCT116 cells were also examined. The results showed that the IC_{50} value of Bu-Lip was 12.35 ± 0.10 ng·mL^{-1}, the IC_{50} value of Ap-Lip was 11.00 ± 0.15 μg·mL^{-1}, and the IC_{50} value of Bu&Ap-Lip was 6.61 ± 0.45 ng·mL^{-1} (Figure S5). The results indicated that after encapsulation by liposomes, the water solubility and bioavailability of the hydrophobic drugs were enhanced.

Preparation and Characterization of Bu&Ap-Lip@IR820 Gel

The phase transition temperature of hydrogels with varying matrix concentrations was determined via the inversion method, establishing the optimal concentration of PLGA-PEG-PLGA as 17.5% (Figure S6). Photothermal conversion experiments and photothermal stability experiments confirmed that the expected photothermal effect could be achieved when the concentration of the photothermal agent IR820 was 0.2 mg·mL^{-1} (Figure S7). The Gel and Bu&Ap-Lip @IR820 gel exhibits good fluidity at 25°C. After being placed at 37 °C for 15 min, they can quickly turn into a non-flowing gel state. When the temperature is further increased to 50 °C, it can return to the flowable sol state again (Figure 2A). The whole transition process from 25 °C to 50 °C is reversible, which indicates that Bu&Ap-Lip@IR820 Gel has good thermosensitive properties and Bu&Ap-Lip and IR820 do not affect the crosslinking of the gel. Bu&Ap-Lip @IR820 Gel was uniformly dispersed and stable in different solutions, and no agglomeration and stratification occurred after 7 days at room temperature (Figure 2B), which proved its good stability. SEM results showed that Bu&Ap-Lip @IR820 Gel exhibited a loose and uniform porous structure with a large number of interconnected pores (Figure 2C). It can be seen from Figure 2D that Gel and Bu&Ap-Lip@IR820 Gel have good injectability, and the injectability is not affected by the addition of Bu&Ap-Lip and IR820. The weight of Gel, Bu&Ap-Lip Gel and Bu&Ap-Lip@IR820 Gel did not change significantly after 24 h immersion in water, which proved that Bu&Ap-Lip@IR820 Gel had no obvious swelling effect, and the addition of Bu&Ap-Lip and IR820 did not affect the safe swelling properties of hydrogels (Figure 2E and F). These results indicate the potential of the obtained hydrogels for in vivo implantation.

https://doi.org/10.2147/IJN.S575430

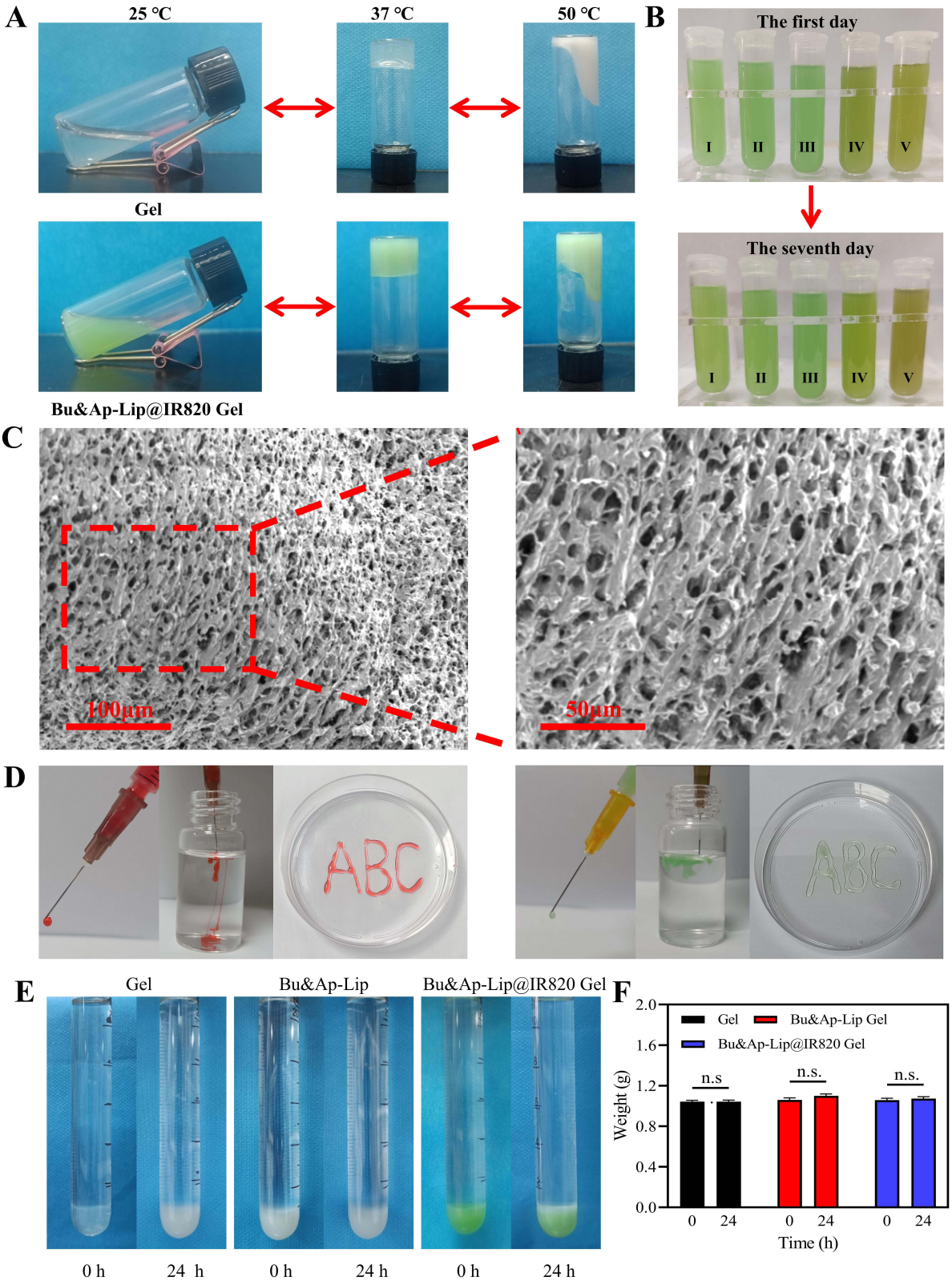

Figure 2 Characterization of Bu&Ap-Lip@IR820 Gel. (**A**) The reversible "sol-gel-sol" transition characteristics of Gel and Bu&Ap-Lip@IR820 Gel. (**B**) Preliminary stability study of Bu&Ap-Lip@IR820 Gel at room temperature (From I to V, purified water, saline, PBS, complete medium, fetal bovine serum). (**C**) SEM images of Bu&Ap-Lip@IR820 Gel. (**D**) Photographs of Gel and Bu&Ap-Lip@IR820 Gel injected into 37 °C water via syringe and writing the letter "ABC". (**E**) Gel, Bu&Ap-Lip Gel and Bu&Ap-Lip@IR820 Gel swelling images. (**F**) The weight changes of Gel, Bu&Ap-Lip Gel and Bu&Ap-Lip@IR820 Gel before and after 24 h.

https://doi.org/10.2147/IJN.S575430

Subsequently, the rheological properties of Bu&Ap-Lip@IR820 Gel were further characterized. The results of temperature scanning experiments showed that the storage modulus (G') and loss modulus (G") of Gel and Bu&Ap-Lip@IR820 Gel showed a "sol-gel" transition at 33 °C, and a reversible "gel-sol" transition occurred with increasing temperature (Figure 3A and B). At 37 °C, Bu&Ap-Lip@IR820 Gel can complete gelation within 34s (Figure 3C). In the frequency scanning experiment, G' is always higher than G" and there is no intersection point (Figure 3D), which proves its good injectability. In the strain range of 0.01% ~ 100%, a wide linear viscoelastic region can be observed, indicating that Bu&Ap-Lip@IR820 Gel can maintain the gel state in a wide strain range (Figure 3E). The self-healing properties of Bu&Ap-Lip@IR820 Gel were studied by cyclic strain scanning experiments. The hydrogel maintained the gel state (G' > G") at small strain and turned to fluid-like behavior (G" > G') at large strain. After multiple damage repairs, the G' value of the hydrogel did not decrease, which proved that Bu&Ap-Lip@IR820 Gel had good self-healing properties (Figure 3F). The reversible test under alternating temperatures indicated that at 37°C, G' > G", and the Bu&Ap-Lip @IR820 Gel was in a gel state; at 45°C, G" > G', and the Bu&Ap-Lip@IR820 Gel was in a sol state (Figure S8). And after three temperature alternations, it still exhibited excellent gel-sol conversion ability.

The real-time images of different hydrogels under laser irradiation are shown in Figure 3G, and the temperature change area is limited to the irradiation point of the gel. The photothermal curves of different gels are shown in Figure 3H, Gel and Bu&Ap-Lip Gel without IR820 have no significant change in temperature under NIR continuous irradiation for 5 min. On the contrary, the temperature of IR820 Gel and Bu&Ap-Lip@IR820 Gel containing IR820 increased rapidly under NIR irradiation, and the temperature exceeded 55 °C. This indicates that Bu&Ap-Lip@IR820 Gel has good photothermal conversion performance. The results of multi-cycle irradiation experiments are shown in Figure 3I, the maximum temperature of Bu&Ap-Lip@IR820 Gel was not attenuated under multiple cycles of irradiation, indicating that Bu&Ap-Lip@IR820 Gel has good photothermal stability. The results of in vitro drug release showed that the cumulative release of Ap from Bu&Ap-Lip@IR820 Gel without NIR irradiation was 57.44% within 48 h, while the cumulative release of Ap reached 81.22% after 2 times of NIR irradiation, and the drug release was significantly increased, which proved that Bu&Ap-Lip@IR820 Gel had photothermal responsive drug controlled-release performance

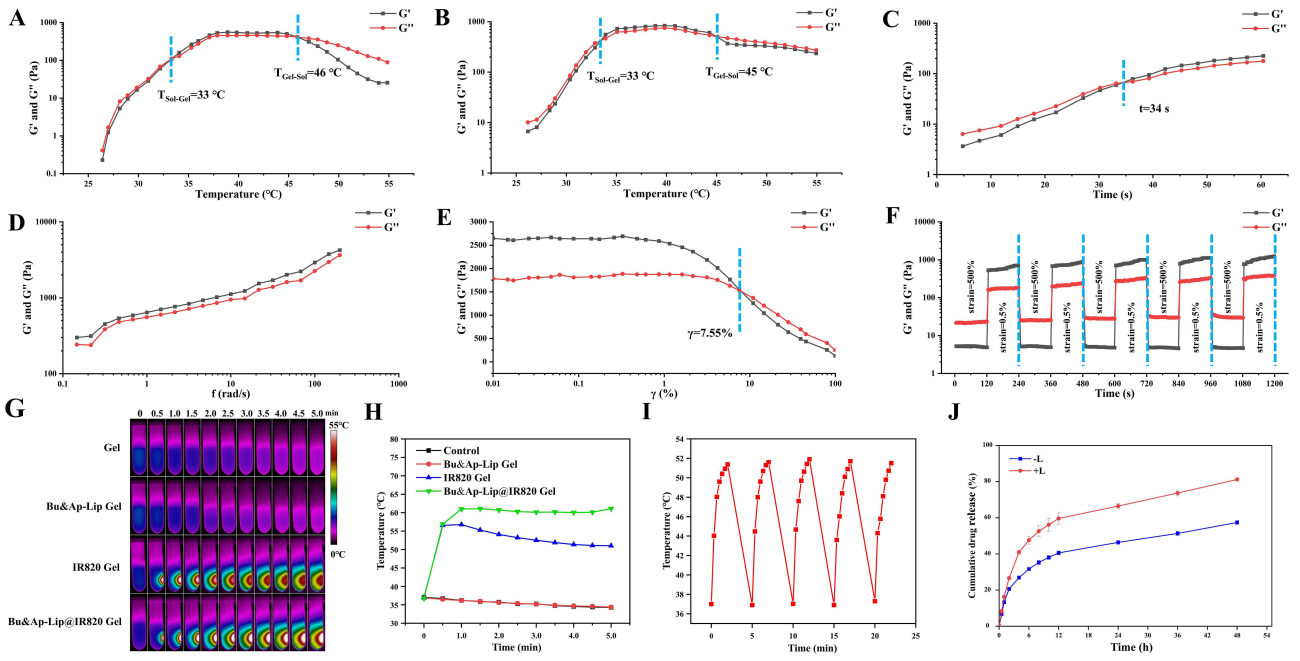

Figure 3 Rheological Properties, Photothermal Performance, and In Vitro Release Characteristics of Bu&Ap-Lip@IR820 Gel. (**A**) The temperature scanning experiment of Gel. (**B**) Temperature scanning experiment of Bu&Ap-Lip@IR820 Gel. (**C**) Isothermal time scanning experiment of Bu&Ap-Lip@IR820 Gel. (**D**) Frequency scanning experiment of Bu&Ap-Lip@IR820 Gel. (**E**) Strain scanning experiment of Bu&Ap-Lip@IR820 Gel. (**F**) Cyclic strain scanning experiment of Bu&Ap-Lip@IR820 Gel. (**G**) Gel, Bu&Ap-Lip Gel, IR820 Gel and Bu&Ap-Lip@IR820 Gel were irradiated with 808 nm (2.5 W·cm^{-2}) laser for different times. (**H**) Time-dependent photothermal curves of Gel, Bu&Ap-Lip Gel, IR820 Gel and Bu&Ap-Lip@IR820 Gel. (**I**) Bu&Ap-Lip@IR820 Gel was irradiated by 808 nm (2.5 W·cm^{-2}) laser for 5 cycles. (**J**) The cumulative release curve of Bu&Ap-Lip@IR820 Gel with or without laser irradiation. G': storage modulus; G": loss modulus.

https://doi.org/10.2147/IJN.S575430

(Figure 3J). Due to the low content of Bu in Bu&Ap-Lip@IR820 Gel, we further investigated the release trend of Bu in the hydrogel after illumination by expanding the concentration of Bu. As shown in Figure S9, the drug release trend is the same at low, medium and high doses, and the drug release increases significantly after illumination. These results indicate that the temperature rise caused by laser irradiation can accelerate the movement of drugs in the liposome-hydrogel system and promote the diffusion of drug molecules outside the gel.

In vitro Biocompatibility of Hydrogels

The survival rate of NCM460 cells cultured in high concentrations (100%) of Gel and Lip@IR820 gel hydrogel extracts exceeded 90%, indicating good cell compatibility (Figure 4A). This proves that the prepared hydrogels and liposomes are

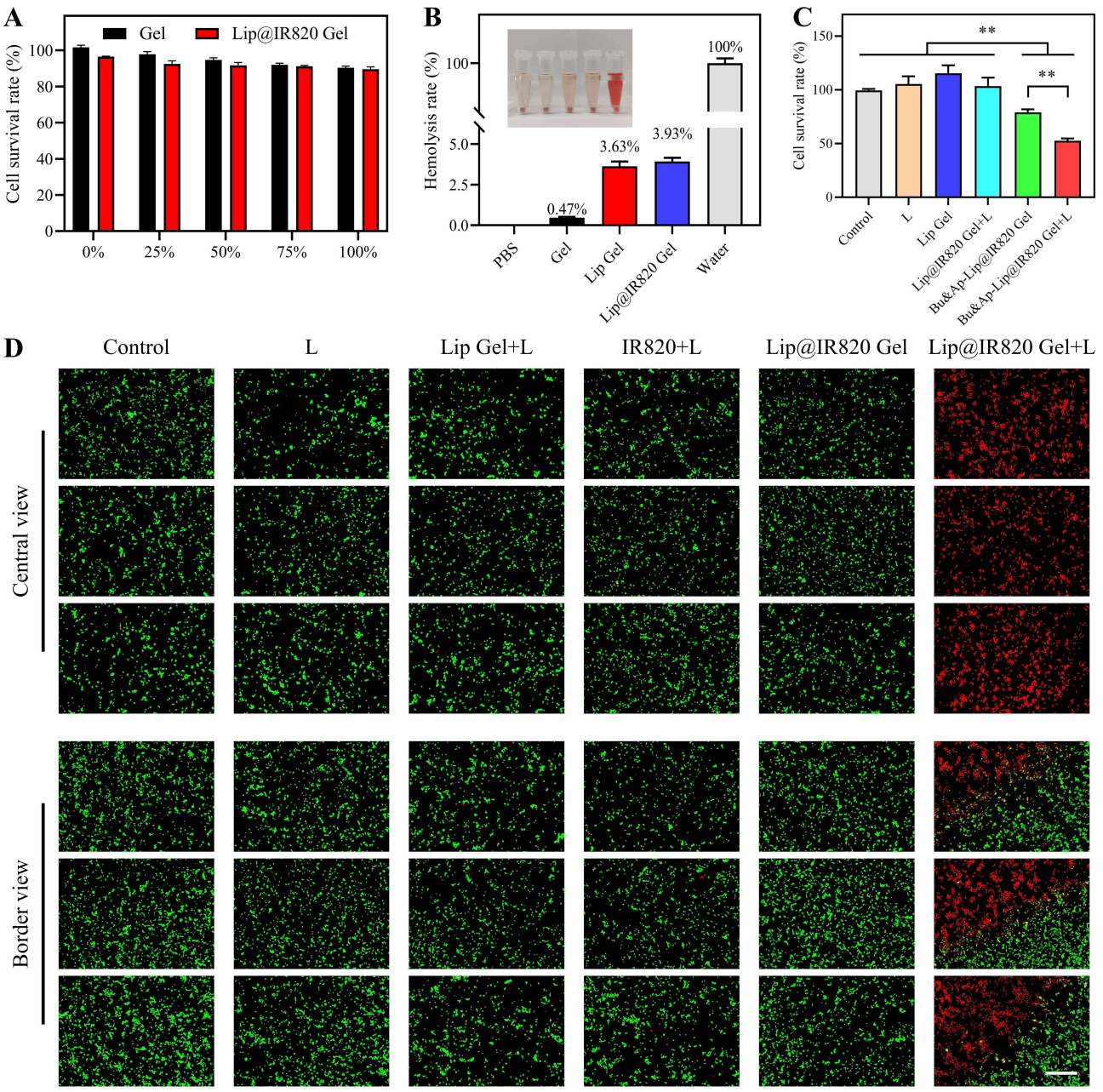

Figure 4 In vitro biocompatibility and photothermal effects. (**A**) The survival rate of NCM460 cells treated with different concentrations of hydrogel extract. (**B**) Hemolysis rate of hydrogel. (**C**) The effect of different drugs on the survival rate of HCT116 cells. (**D**) Images of live and dead cell staining results of HCT116 cells treated with different drugs. Scale bar: 500 μm. (n = 3, $^{**}p < 0.01$).

safe and non-toxic. As shown in Figure 4B, compared with the hemolysis rate of Water (100%), the hemolysis rates of Gel, Lip Gel and Lip@IR820 were 0.47%, 3.63% and 3.93%, respectively, and the hemolysis rates were less than 5.0%, indicating that the prepared hydrogels and liposomes have good blood compatibility.

In vitro Antitumor Activity of Bu&Ap-Lip@IR820 Gel

In vitro Cytotoxicity

The in vitro antitumor effects of Bu&Ap-Lip@IR820 Gel were evaluated using the MTT assay, with results shown in Figure 4C. Compared with the blank group (100%), the tumor cell survival rates in the Bu&Ap-Lip@IR820 Gel and Bu&Ap-Lip@IR820 Gel + L groups decreased by 21.19% and 47.50%, respectively, both demonstrating strong cytotoxic effects. The cell survival rate of the Bu&Ap-Lip@IR820 Gel + L group was the lowest. This is because the localized high heat generated by laser irradiation promotes the release of more Bu and Ap from Bu&Ap-Lip@IR820 Gel, thereby inducing more tumor cell death.

In vitro Photothermal Effect

The photothermal effect of IR820 in vitro was investigated by live-dead staining experiments. There was no obvious red fluorescence in the IR820 + L group, showing a weak tumor killing effect. In the Lip@IR820 Gel + L group, the central area near the bottom of the cell culture plate from the upper chamber of the transwell showed strong red fluorescence, the edge area showed green fluorescence, and the central area showed a strong tumor cell killing effect (Figure 4D). The results of the cell apoptosis experiment showed that the apoptosis rate in the Lip@IR820 Gel + L group was significantly higher than that in the other groups (Figure S10). The results show that the hydrogel can prolong the local retention time of IR820, thereby maintaining a high concentration locally and generating a good photothermal effect, which effectively induces cell apoptosis.

Cell Apoptosis Assay

The results of apoptosis are shown in Figure 5A. Compared with the control group, the apoptosis rates of the Bu&Ap-Lip @IR820 Gel and Bu&Ap-Lip@IR820 Gel + L groups increased by 37.03% and 56.06%, respectively, significantly promoting apoptosis in HCT116 cells. Compared with the Bu&Ap-Lip@IR820 Gel group, the Bu&Ap-Lip@IR820 Gel + L group showed a 19.03% increase in apoptosis rate, demonstrating stronger pro-apoptotic activity.

Cell Migration Assay

The effects of different drugs on the migration ability of tumor cells were evaluated by scratch healing experiments. The results are shown in Figure 5B. Compared with the control group, the relative migration rates of Bu&Ap-Lip@IR820 Gel and Bu&Ap-Lip@IR820 Gel + L groups decreased by 18.25% and 30.84%, respectively, indicating that cell migration was inhibited. Compared with the Bu&Ap-Lip@IR820 Gel group, the relative cell migration rate of Bu&Ap-Lip@IR820 Gel + L group decreased by 12.59%, which indicated that the migration ability of tumor cells was further inhibited.

Cell Invasion Assay

The effects of different drugs on the invasion ability of tumor cells were evaluated by the transwell assay. As shown in Figure 5C, compared with the control group, the number of invasive cells in the Bu&Ap-Lip@IR820 Gel and Bu&Ap-Lip@IR820 Gel + L groups decreased by 4699 and 8468, respectively, indicating that cell invasion was inhibited. Compared with the Bu&Ap-Lip@IR820 Gel group, the number of invasive cells in Bu&Ap-Lip@IR820 Gel + L group decreased by 3769, which indicated that the invasion ability of tumor cells was further inhibited.

HUVCE Tubule Formation Assay

The results of the HUVCE tube formation assay are shown in Figure 5D. Compared with the blank group, the number of tube branches in the Bu&Ap-Lip@IR820 Gel and Bu&Ap-Lip@IR820 Gel + L groups decreased by 53 and 107, respectively, indicating that angiogenesis was inhibited. The number of tube branches in the Bu&Ap-Lip@IR820 Gel +L group was significantly reduced. The localized high heat induced by NIR irradiation promoted the release of more Bu and Ap from the Bu&Ap-Lip@IR820 Gel, thereby exerting a stronger inhibitory effect on angiogenesis.

https://doi.org/10.2147/IJN.S575430

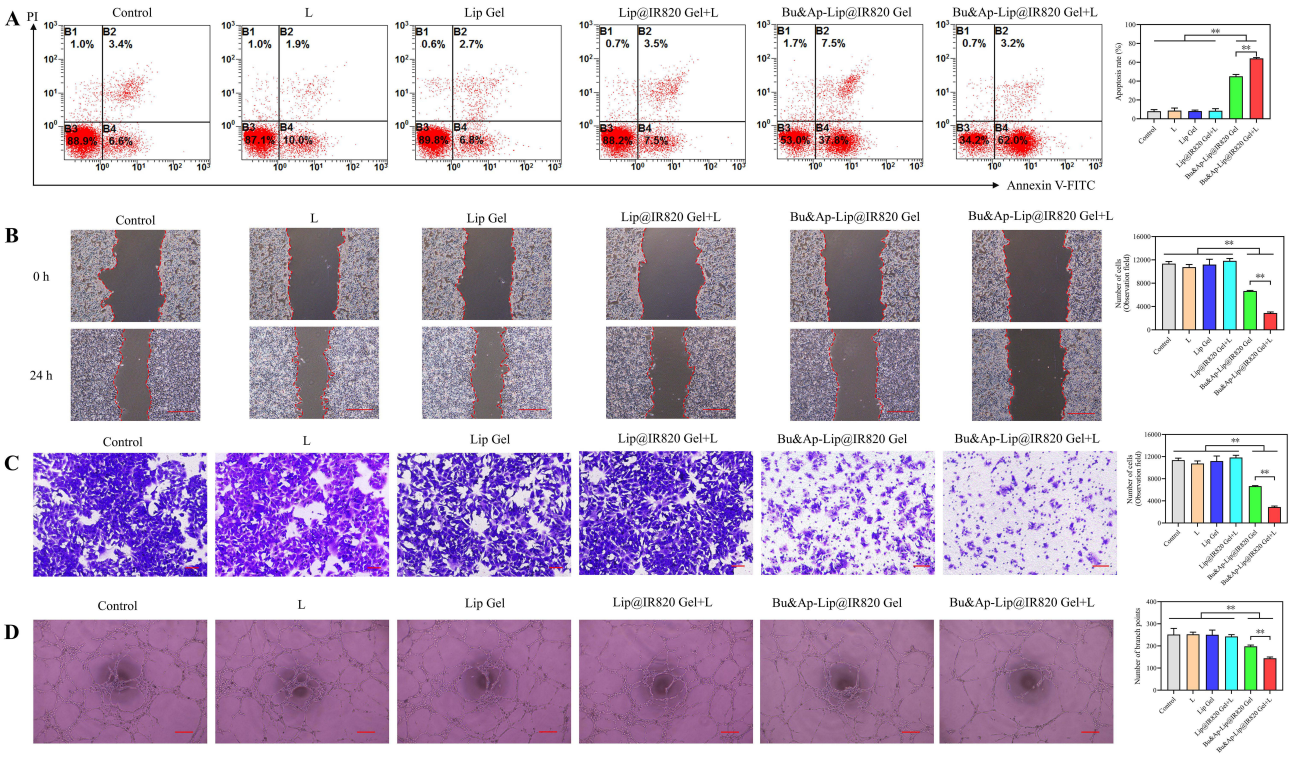

Figure 5 Mechanism of In Vitro Antitumor Activity of Bu&Ap-Lip@IR820 Gel. (**A**) Effect of different drugs on the apoptosis rate of HCT116 cells. (**B**) Anti-migration effect of different drugs on HCT116 cells. Scale bar: 500 μm. (**C**) Anti-invasion effect of different drugs on HCT116 cells. Scale bar: 100 μm. (**D**) Effect of different drugs on HUVEC angiogenesis. Scale bar: 100 μm. (n = 3, $^{**}p < 0.01$).

Western Blot

To further investigate the antitumor mechanism of Bu&Ap-Lip@IR820 Gel + L, Western blotting was used to quantitatively detect the expression of relevant proteins. As shown in Figure 6A and B, Cleaved Caspase-3 expression was elevated, while Ki-67, VEGF, MMP-2, and CD31 expression was reduced in the Bu&Ap-Lip@IR820 Gel and Bu&Ap-Lip@IR820 Gel + L groups. The Bu&Ap-Lip@IR820 Gel + L group showed the most significant effect, further confirming that the Bu&Ap-Lip@IR820 Gel group, after NIR laser irradiation, can induce local hyperthermia, thereby releasing more Ap and Bu, significantly increasing the expression of Cleaved Caspase-3 in HCT116 cells, and reducing the expression of Ki-67, MMP-2, VEGF, and CD31 expression, thereby exerting an anti-colon cancer effect.

In vivo Anti-Tumor Recurrence Effect

In vivo Biocompatibility and Retention of Bu&Ap-Lip@IR820 Gel

Bu&Ap-Lip@IR820 Gel was subcutaneously injected into nude mice to investigate the in vivo biocompatibility of the hydrogel. The results showed that during the observation period, the skin around the injection site was normal without swelling or redness. The histopathological examination results of HE staining are shown in Figure 7A. There were no obvious pathological changes around the injection site, indicating that the Bu&Ap-Lip@IR820 Gel had good biocompatibility. The drug release performance of the hydrogel in vivo was monitored by the IVIS system. The results are shown in Figure 7B. The fluorescence signal can be detected in the DiD group on the first day, and the fluorescence signal disappears on the seventh day, indicating that the free DiD is easily diffused or degraded rapidly in the body. The fluorescence intensity of DiD-Lip@IR820 Gel group fluorescence signals can be detected throughout the monitoring period (Figure 7C), which indicates that the liposome hydrogel can slowly release the loaded drug and maintain stable and long-term drug concentration in the body for long-term treatment. Compared with the DiD-Lip@IR820 Gel group, the fluorescence intensity of the DiD-Lip@IR820 Gel + L group was significantly reduced after 2 times of NIR laser

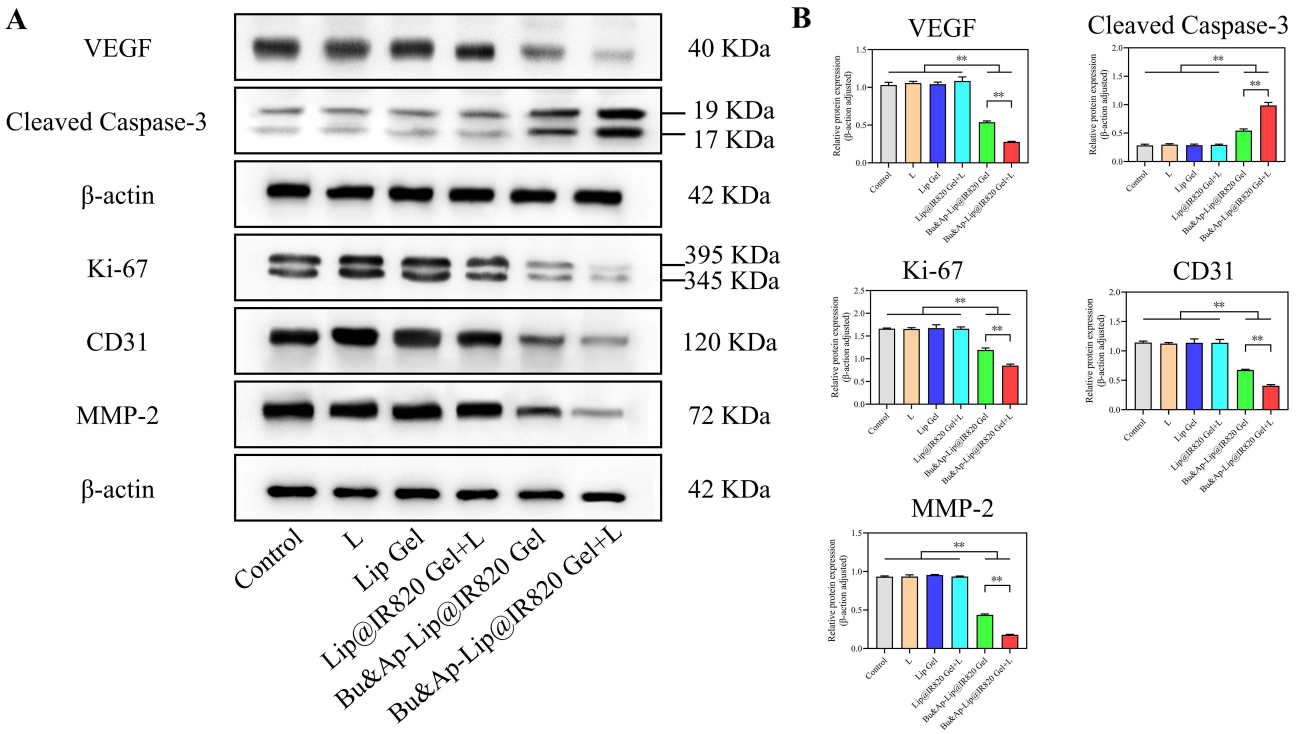

Figure 6 Multipathway protein modulation in HCT116 cells by photothermal-responsive hydrogel system. (**A**) WB was used to detect the effects of different drugs on Ki-67, Cleaved Caspase-3, MMP-2, VEGF and CD31 proteins in HCT116 cells. (**B**) Histogram of Ki-67, Cleaved Caspase-3, MMP-2, VEGF and CD31 expression in HCT116 cells. (n = 3, $^{**}p < 0.01$).

irradiation. On the 14th day, only weak fluorescence signals were detected, indicating that the prepared hydrogel can intelligently adjust the release of the loaded therapeutic agent by turning on/off the NIR laser.

In vivo Photothermal Effect of Bu&Ap-Lip@IR820 Gel

In vivo photothermal experiments are shown in Figure 7D and E. Under the irradiation of 808 nm (2.5 $W \cdot cm^{-2}$) NIR laser, the temperature of the injection site was maintained at about 37 °C and there was no significant change in the saline group and the Lip Gel group. Lip@IR820 Gel and Bu&Ap-Lip@IR820 Gel + L groups were irradiated by 808 nm (2.5 $W \cdot cm^{-2}$) NIR laser. The temperature of the injection site rapidly reached about 52 °C within 1 min of irradiation, and then remained at about 52 °C, which was enough to kill tumor cells and promote the release of the loaded drug. These results indicate that Bu&Ap-Lip@IR820 Gel has good and stable in vivo photothermal properties.

The Anti-Tumor Recurrence Effect of Bu&Ap-Lip@IR820 Gel

The in vivo experimental design of Bu&Ap-Lip@IR820 Gel for preventing tumor recurrence is shown in Figure 8A, and the procedure is performed as illustrated in Figure 8B. The IVIS monitoring results of tumor recurrence after surgery are displayed in Figure 8C. Tumor recurrence appeared earlier and progressed rapidly in the saline, Bu + Ap, and Lip Gel groups, with strong fluorescence signals observed on day 7. In contrast, the Lip@IR820 Gel + L, Bu&Ap-Lip@IR820 Gel, and Bu&Ap-Lip@IR820 Gel + L groups showed a decrease or even disappearance of fluorescence intensity in the later stages of the experiment, indicating that tumor development was inhibited or even eliminated. The tumor photos removed after 28 days were monitored as Figure 8D, and the tumor recurrence inhibition rate was calculated as Figure 8E. The tumor recurrence inhibition rates of saline, Bu + Ap, Lip Gel, Lip@IR820 Gel + L, Bu&Ap-Lip @IR820 Gel and Bu&Ap-Lip@IR820 Gel + L groups were 0.00%, 16.67%, 0.00%, 16.67%, 8.33% and 66.67%, respectively. The results showed that the Bu&Ap-Lip@IR820 Gel + L group showed a more efficient anti-tumor recurrence effect. At the same time, the Bu&Ap-Lip@IR820 Gel + L group showed the lightest tumor weight (Figure 8F). In conclusion, the Bu&Ap-Lip@IR820 Gel + L group has the best anti-tumor recurrence effect, which may be due to the photothermal ablation and photothermal triggering of Bu and Ap release by Bu&Ap-Lip@IR820 Gel

https://doi.org/10.2147/IJN.S575430

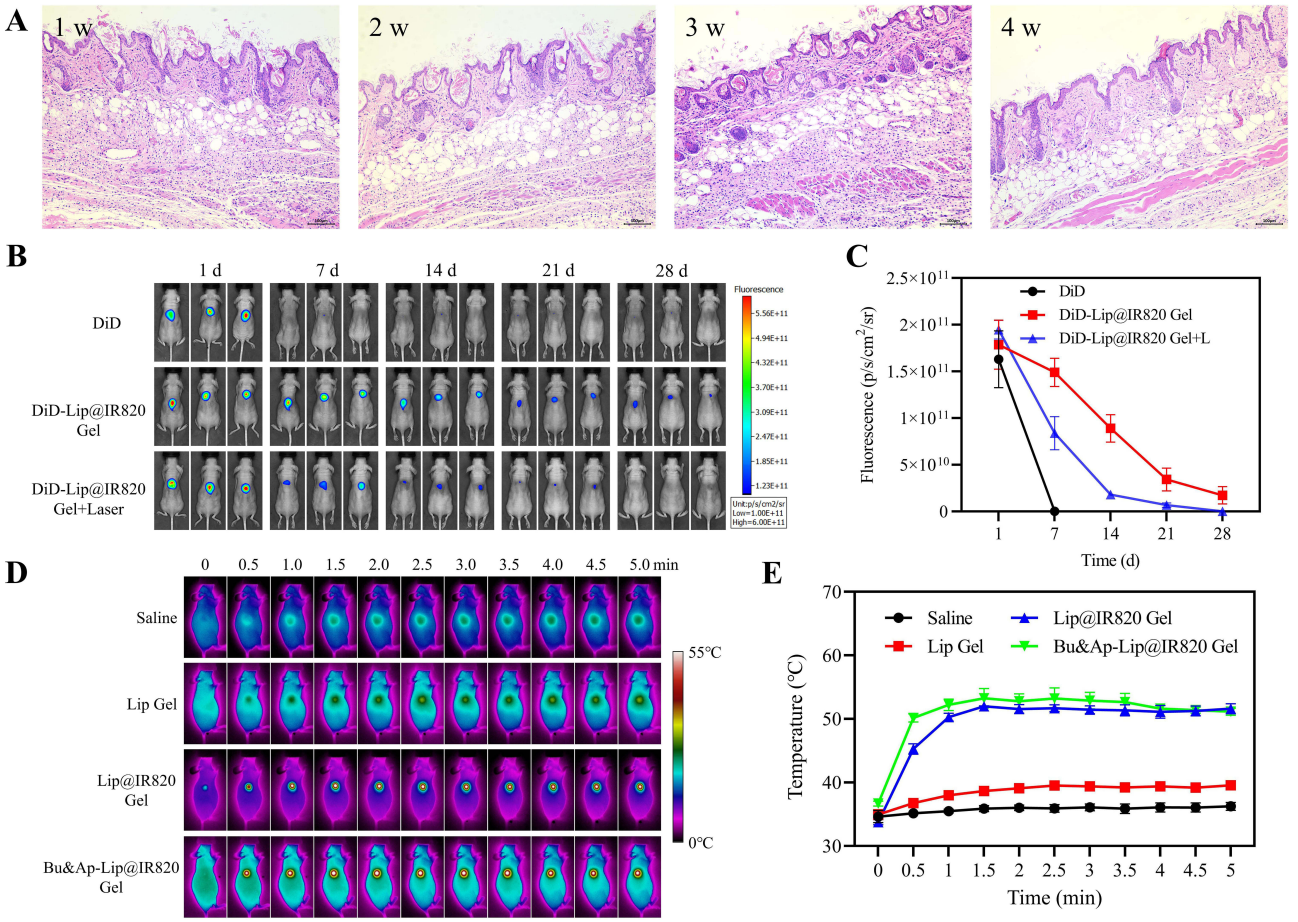

Figure 7 In vivo retention of hydrogels and their photothermal effects. (**A**) HE staining results of subcutaneous tissue at different time points (n=3). Scale bar: 100 μm. (**B**) DiD as a fluorescent marker and IVIS system were used to record the fluorescence images of the back of nude mice injected with different preparations (n=3). (**C**) Semi-quantitative analysis of fluorescence intensity. (**D**) Thermal imaging images of different drugs after subcutaneous injection with 808 nm laser continuous irradiation for 5 min (n=3). (**E**) Temperature curves of different drugs over time.

under NIR laser irradiation, which greatly improves its inhibitory effect on postoperative tumor recurrence and metastasis. No significant weight loss was observed in all treatment groups throughout the monitoring period except for decreased postoperative comfort (Figure 8G).

To further investigate the anti-tumor recurrence mechanism of Bu&Ap-Lip@IR820 Gel + L, we conducted additional analyses on tumor tissues from each group. HE staining revealed severe tumor necrosis in the Bu&Ap-Lip@IR820 Gel + L group, with irregularly arranged tumor cells and a significant reduction in tumor cell density. We also performed immunohistochemical analysis to assess the expression of four proteins, Ki-67, Cleaved Caspase-3, MMP-2, and VEGF in the tumor tissues. The results showed that the Bu&Ap-Lip@IR820 Gel + L group had the highest expression of Cleaved Caspase-3 and the lowest expression of Ki-67, MMP-2, and VEGF (Figure S11A–D). TUNEL assay results showed the strongest green fluorescence staining in the Bu&Ap-Lip@IR820 Gel + L group, indicating the highest number of apoptotic cells (Figure S11E). Additionally, immunofluorescence analysis was performed to assess CD31 protein expression in tumor tissues. Results showed the weakest red fluorescence in the Bu&Ap-Lip@IR820 Gel + L group, indicating the lowest CD31 expression and the strongest anti-angiogenic effect (Figures 9 and S11F). In addition to no weight loss during treatment, the main organs of nude mice in each treatment group were subjected to HE staining (Figure S12), and biochemical indicators in blood samples (Figure S13A and B) were measured. Compared with the physiological saline control group, Bu&Ap-Lip@IR820 gel treatment had no significant effect on blood or organs. These results indicate that Bu&Ap-Lip@IR820 gel has good biosafety at this dose.

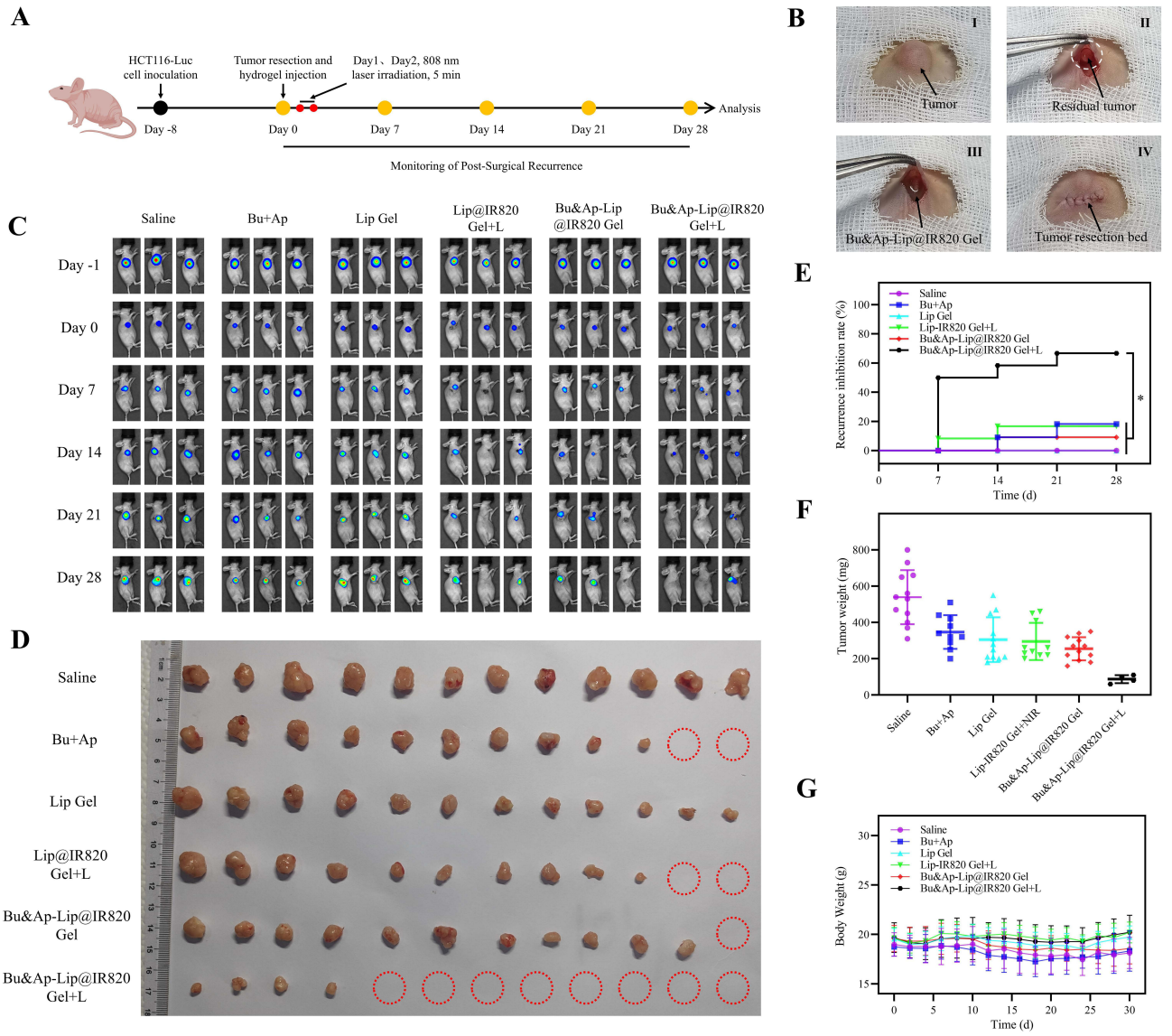

Figure 8 Efficacy of hydrogel in inhibiting postoperative recurrence of tumor in vivo. (**A**) Operation steps of hydrogel in inhibiting postoperative recurrence. (**B**) Tumor resection and hydrogel platform injection process. (**C**) IVIS monitoring postoperative recurrence of the tumor. (**D**) Image of tumor resection (n=12, The red circle indicates complete tumor suppression.). (**E**) Tumor recurrence inhibition rate (n=12). (**F**) Tumor weight of mice after different treatments. (**G**) Weight of mice treated with different drugs (n=12). *$p < 0.05$.

Discussion

Colon cancer is the most common malignant tumor of the digestive system in the world. Postoperative tumor recurrence is one of the core causes of death in patients with colon cancer. Postoperative adjuvant chemotherapy is the main way to inhibit the recurrence of colon cancer, but long-term use can easily lead to immune system damage, multidrug resistance and serious adverse reactions. In recent years, traditional Chinese medicine treatment has shown unique advantages in the clinical treatment of malignant tumors. Bu is one of the main active components of dried toad skin, a traditional Chinese medicine. It can effectively inhibit the recurrence and metastasis of colon cancer by inducing apoptosis and cycle arrest, inhibiting cell invasion and metastasis, reversing multidrug resistance, and regulating multiple signaling pathways. Ap is a small molecule tyrosine kinase inhibitor with high selectivity and inhibition of VEGFR-2. It can inhibit tumor cell growth by inhibiting angiogenesis and reducing the microvascular density of tumor cells. IR820 is a NIR dye with high photothermal conversion efficiency, light stability and low photobleaching performance. Related studies have shown that IR820-mediated PTT has a good anti-tumor recurrence effect on a variety of malignant tumors. In summary, Bu, Ap, and

https://doi.org/10.2147/IJN.S575430

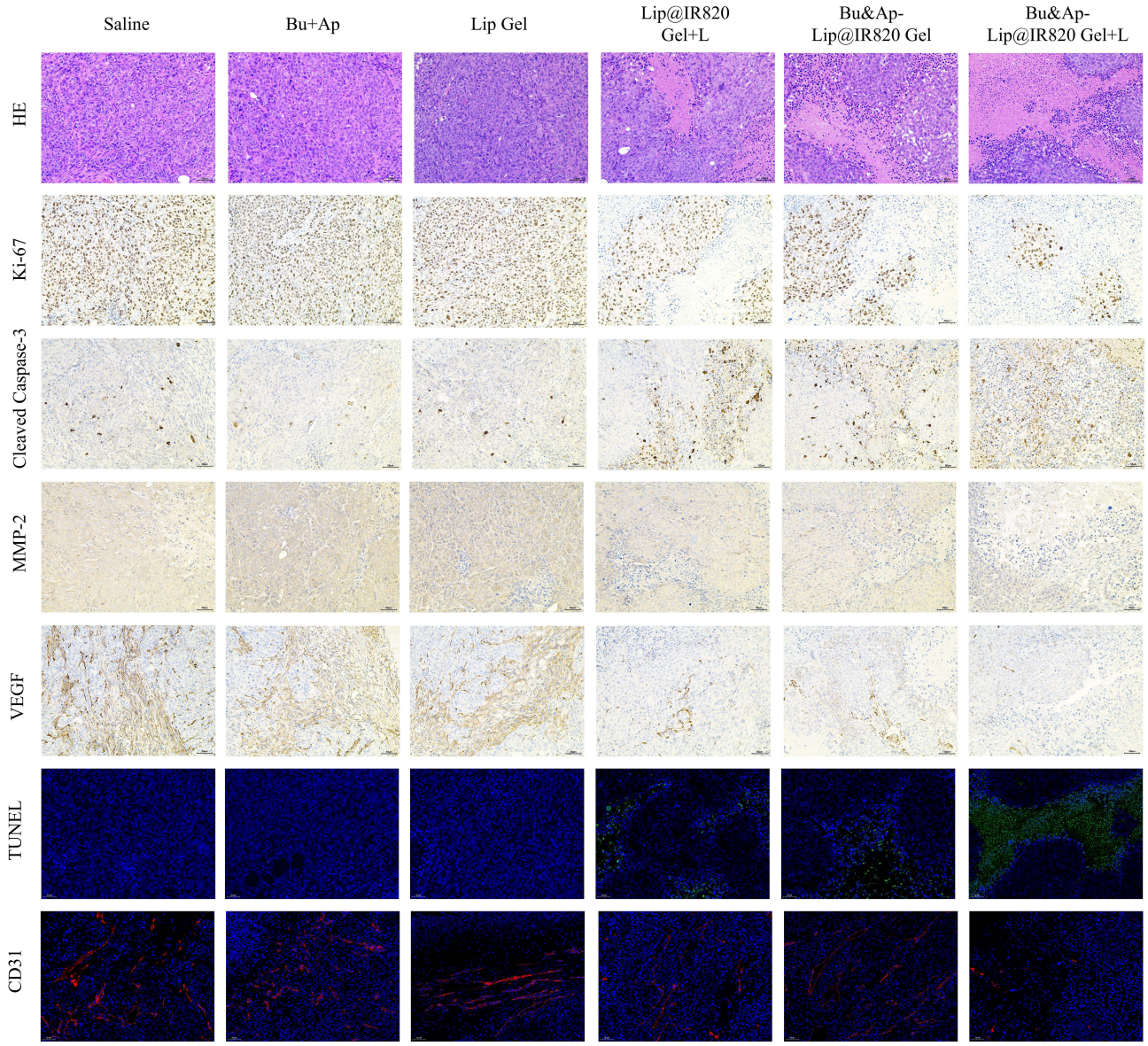

Figure 9 Study on the Antitumor Effects of Bu&Ap-Lip@IR820 Gel in vivo. HE, Ki-67, Cleaved Caspase-3, MMP-2, VEGF, TUNEL, and CD31 staining images of tumor tissue (n=3). Scale bar: 50 μm.

IR820 demonstrate significant efficacy in the treatment of colon cancer. However, Bu has the drawback of strong cardiac toxicity, Ap has low oral bioavailability, and the photosensitizer IR820 has weak tumor targeting ability. Based on this, this study developed an in situ injectable thermosensitive liposome hydrogel. By encapsulating the three drugs in the same hydrogel platform, the issues associated with Bu, Ap, and IR820 in tumor treatment were overcome, and the controlled release of drugs could be achieved through local photothermal response, thereby synergistically preventing tumor recurrence.

In this study, the synergistic ratio of Bu and Ap on HCT116 cells was first investigated. The results showed that when the mass ratio (ng/μg) of Bu and Ap was 2: 1, the CI value was the smallest and the drug synergistic effect was the strongest. The special amphiphilic closed vesicle structure of liposomes makes it possible to effectively solve the problem of poor water solubility and improve the bioavailability of Bu and Ap, and the application of thermosensitive liposome materials can achieve controlled release of drugs through thermal response. DPPC is a commonly used phospholipid material for preparing thermosensitive liposomes. The addition of a certain amount of MSPC during

preparation can not only make the prepared thermosensitive liposomes obtain more stable drug release pores when they become a flowing state, but also reduce the phase transition temperature of thermosensitive liposomes and reduce the damage of high temperature to normal tissues. On this basis, DSPE-PEG_{2000} is added to prolong the circulation time in vivo by reducing the repulsion between polymers.[47,48] Therefore, in this study, DPPC, MSPC and DSPE-PEG_{2000} were selected as the membrane materials, and the thermosensitive liposomes (Bu&Ap-Lip) encapsulating Bu and Ap were prepared by the thin film dispersion method. The best preparation prescription and process of Bu&Ap-Lip were optimized by a single-factor experiment combined with Box-Behnken. Bu&Ap-Lip exhibits excellent dispersibility, stability, and thermosensitive drug release properties. PLGA-PEG-PLGA is a triblock, injectable, temperature-sensitive hydrogel with good biocompatibility and biodegradability.[49] This study obtained Bu&Ap-Lip@IR820 Gel by mixing PLGA-PEG-PLGA with Bu&Ap-Lip and IR820, followed by thorough swelling. This study proves that Bu&Ap-Lip @IR820 Gel has excellent "sol-gel-sol" phase transition conversion performance, which can be rapidly gel at physiological temperature, and then can be converted into a flowable sol when the temperature increases. Bu&Ap-Lip@IR820 Gel showed a loose and uniform porous structure under SEM, with good injectability, gel properties, photothermal properties and swelling properties. Additionally, Bu&Ap-Lip@IR820 Gel enables light-controlled drug release through IR820-mediated photothermal response.

In vitro studies indicate that Bu&Ap-Lip@IR820 Gel exhibits potent cytotoxicity against HCT116 cells under near-infrared light irradiation, significantly inducing apoptosis while inhibiting cell migration and invasion. Concurrently, Bu&Ap-Lip@IR820 Gel effectively suppresses the tube-forming capacity of HUVEC cells, demonstrating its anti-angiogenic activity. Further protein expression analysis revealed that Bu&Ap-Lip@IR820 Gel mechanism of action is closely associated with the upregulation of Cleaved Caspase-3 and the downregulation of key proteins such as Ki-67, MMP-2, VEGF, and CD31. This demonstrates that Bu&Ap-Lip@IR820 Gel exerts its antitumor effects through a multi-pathway synergistic mechanism. Finally, we studied the anti-tumor recurrence effect and mechanism of Bu&Ap-Lip @IR820 Gel in vivo. Firstly, it was proved that the hydrogel had good biocompatibility and retention in vivo. HCT116-Luc cells were used to establish a postoperative resection model of colon cancer in BALB/c nude mice. IVIS monitoring results showed that Bu&Ap-Lip@IR820 Gel + L group had the strongest anti-tumor recurrence effect. Histological analysis indicates that Bu&Ap-Lip@IR820 Gel promotes tumor cell apoptosis and necrosis while downregulating the expression of markers associated with proliferation, invasion, and angiogenesis. Furthermore, Bu&Ap-Lip@IR820 Gel did not induce significant systemic toxicity or organ damage at therapeutic doses, confirming its excellent biosafety profile.

This study successfully developed Bu&Ap-Lip@IR820 Gel, achieving safe and efficient inhibition of colon cancer recurrence after surgery through light-responsive drug release. While our results demonstrate the promise of this combined strategy, we acknowledge several limitations of the present study that point to directions for future research. First, this study confirmed the synergistic antitumor effects of Bu and Ap through the CI. However, the regulatory mechanisms underlying their synergistic interaction have yet to be systematically elucidated at the molecular level. In subsequent studies, we will comprehensively elucidate the molecular mechanisms underlying the synergistic antitumor effects of Bu and Ap through transcriptomics, pathway enrichment analysis, and targeted validation of key signaling cascades such as the STAT3 and PI3K/AKT/mTOR pathways. In experimental design, this study focused on validating the overall efficacy of the integrated strategy "local delivery + photothermal triggering + multimodal synergy" and thus did not establish complete controls for all individual groups. This limitation partially constrained the verification of the independent antitumor mechanisms of each treatment modality. Additionally, in vitro photothermal efficacy assessments were limited to flow cytometric quantification of apoptosis. Future studies will dynamically correlate temperature elevation with apoptosis molecular markers. Postoperative recurrence models lacked analysis of residual tumor survival rates and phenotypes; addressing these gaps will enhance the model's clinical relevance. Finally, while this study indirectly demonstrated the excellent local retention and controlled release properties of Bu&Ap-Lip@IR820 Gel through in vivo fluorescence imaging, pharmacodynamic, and systemic safety evaluations, quantitative data on the pharmacokinetics and biodistribution of the released drug are lacking. Future research will supplement these pharmacokinetic studies to more comprehensively assess the in vivo effects and clinical translation potential of this system.

Conclusion

In conclusion, this study successfully prepared a NIR-responsive injectable composite liposome hydrogel system (Bu&Ap-Lip@IR820 Gel). This system could achieve local precise drug delivery through "sol-gel-sol" transformation and photocontrolled drug release characteristics. This system could also efficiently inhibit the postoperative recurrence of colon cancer through synergistically integrating the multi-target anti-tumor properties of Bu, the targeted inhibitory effect of Ap on tumor angiogenesis and the photothermal therapeutic advantages of IR820 with good biocompatibility and biosafety, which provides a novel strategy for clinical postoperative anti-recurrence treatment of colon cancer.

Consent for Publication

All authors agree to publication.

Funding

This research was supported by grants from National Natural Science Foundation of China (grant No. 82204935), The Disciplinary Innovation Team Construction Project of Shaanxi University of Chinese Medicine (2019-YL11), Project of Qinchuangyuan Traditional Chinese Medicine Industry Innovation Aggregation Zone (L2024-QCY-ZYYJJQ-X27; L2024-QCY-ZYYJJQ-X30), Key Research and Development Programme of Shaanxi Province (2025SF-YBXM-493), Project of Xi'an Municipal Health Commission (2025qn01). This study was also supported by the construction project of Zhao Feng National Old Pharmacist Inheritance Studio of State Administration of Traditional Chinese Medicine (National Traditional Chinese Medicine Education Letter [2024]255).

Disclosure

The authors declare no competing interests in this work.

References

1. Bray F, Laversanne M, Sung H, et al. Global cancer statistics 2022: globocan estimates of incidence and mortality worldwide for 36 cancers in 185 countries. *CA Cancer J Clinicians*. 2024;74(3):229–263. doi:10.3322/caac.21834
2. Huang X, Han X, Li W, et al. Case report: a clinical report of photodynamic neoadjuvant combined with fluorescent laparoscopic localization robotic surgery for the treatment of patients with advanced colorectal cancer combined with obstruction. *Front Immunol*. 2024;15:1403613. doi:10.3389/fimmu.2024.1403613
3. Guraya SY. Pattern, stage, and time of recurrent colorectal cancer after curative surgery. *Clin Colorectal Cancer*. 2019;18(2):e223–e228. doi:10.1016/j.clcc.2019.01.003
4. Nors J, Iversen LH, Erichsen R, Gotschalck KA, Andersen CL. Incidence of recurrence and time to recurrence in stage i to iii colorectal cancer: a nationwide Danish cohort study. *JAMA Oncol*. 2024;10(1):54–62. doi:10.1001/jamaoncol.2023.5098
5. Sung H, Ferlay J, Siegel RL, et al. Global cancer statistics 2020: globocan estimates of incidence and mortality worldwide for 36 cancers in 185 countries. *CA Cancer J Clin*. 2021;71(3):209–249. doi:10.3322/caac.21660
6. Arafat Y, Loft M, Cao K, et al. Current colorectal cancer chemotherapy dosing limitations and novel assessments to personalize treatments. *ANZ J Surg*. 2022;92(11):2784–2785. doi:10.1111/ans.18046
7. Han HS, Choi KY. Advances in nanomaterial-mediated photothermal cancer therapies: toward clinical applications. *Biomedicines*. 2021;9(3):305. doi:10.3390/biomedicines9030305
8. Hu J, Cheng Y, Zhang X. Recent advances in nanomaterials for enhanced photothermal therapy of tumors. *Nanoscale*. 2018;10(48):22657–22672. doi:10.1039/c8nr07627h
9. Chen P, Wang X, Zhu C, Guo T, Wang C, Ying L. Targeted delivery of quinoxaline-based semiconducting polymers for tumor photothermal therapy. *ACS Appl Mater Interfaces*. 2024;16(29):38377–38386. doi:10.1021/acsami.4c05668
10. Thirumurugan S, Ramanathan S, Muthiah KS, et al. Inorganic nanoparticles for photothermal treatment of cancer. *J Mater Chem B*. 2024;12(15):3569–3593. doi:10.1039/d3tb02797j
11. Shen S, Qiu J, Huo D, Xia Y. Nanomaterial-enabled photothermal heating and its use for cancer therapy via localized hyperthermia. *Small*. 2024;20(7):e2305426. doi:10.1002/smll.202305426
12. Ma N, Yan Z. Research progress of thermosensitive hydrogel in tumor therapeutic. *Nanoscale Res Lett*. 2021;16(1):42. doi:10.1186/s11671-021-03502-5
13. Zaharie-Butucel D, Potara M, Suarasan S, Licarete E, Astilean S. Efficient combined near-infrared-triggered therapy: phototherapy over chemotherapy in chitosan-reduced graphene oxide-ir820 dye-doxorubicin nanoplatforms. *J Colloid Interface Sci*. 2019;552:218–229. doi:10.1016/j.jcis.2019.05.050
14. Liu G, Ma R, Liu P, Wang K, Cai K. An injectable nanocomposite hydrogel prevents postoperative tumor recurrence and wound infection via synergistic photothermal-chemo-therapy. *J Colloid Interface Sci*. 2024;655:809–821. doi:10.1016/j.jcis.2023.11.066
15. Dash BS, Das S, Chen J. Photosensitizer-functionalized nanocomposites for light-activated cancer theranostics. *Int J Mol Sci*. 2021;22(13):6658. doi:10.3390/ijms22136658

16. Hu X, Tian H, Jiang W, Song A, Li Z, Luan Y. Rational design of ir820- and ce6-based versatile micelle for single nir laser-induced imaging and dual-modal phototherapy. *Small*. 2018;14(52):e1802994. doi:10.1002/smll.201802994
17. Yang X, Gao L, Wei Y, et al. Photothermal hydrogel platform for prevention of post-surgical tumor recurrence and improving breast reconstruction. *J Nanobiotechnol*. 2021;19(1):307. doi:10.1186/s12951-021-01041-w
18. Wu B, Wan B, Lu S, et al. Near-infrared light-triggered theranostics for tumor-specific enhanced multimodal imaging and photothermal therapy. *Int J Nanomed*. 2017;12:4467–4478. doi:10.2147/IJN.S137835
19. Deng K, Tian H, Zhang T, et al. Chemo-photothermal nanoplatform with diselenide as the key for ferroptosis in colorectal cancer. *J Control Release*. 2024;366:684–693. doi:10.1016/j.jconrel.2024.01.024
20. Wang H, Gou R, Chen J, et al. Catalase-positive staphylococcus epidermidis based cryo-millineedle platform facilitates the photo-immunotherapy against colorectal cancer via hypoxia improvement. *J Colloid Interface Sci*. 2024;676:506–520. doi:10.1016/j.jcis.2024.07.145
21. Liu S, Wu F, Zhang Y, et al. Apatinib combined with radiotherapy enhances antitumor effects in an in vivo nasopharyngeal carcinoma model. *Cancer Control*. 2020;27(1):544332511. doi:10.1177/1073274820922553
22. Yang Z, Zhang X, Bai X, Xi X, Liu W, Zhong W. Anti-angiogenesis in colorectal cancer therapy. *Cancer Sci*. 2024;115(3):734–751. doi:10.1111/cas.16063
23. Riccardi C, Napolitano E, Platella C, Musumeci D, Melone MAB, Montesarchio D. Anti-vegf dna-based aptamers in cancer therapeutics and diagnostics. *Med Res Rev*. 2021;41(1):464–506. doi:10.1002/med.21737
24. Li A, Wang K, Xu A, et al. Apatinib as an optional treatment in metastatic colorectal cancer. *Medicine*. 2019;98(35):e16919. doi:10.1097/MD.0000000000016919
25. Cheng X, Feng H, Wu H, et al. Targeting autophagy enhances apatinib-induced apoptosis via endoplasmic reticulum stress for human colorectal cancer. *Cancer Lett*. 2018;431:105–114. doi:10.1016/j.canlet.2018.05.046
26. Feng H, Cheng X, Kuang J, et al. Apatinib-induced protective autophagy and apoptosis through the akt-mtor pathway in anaplastic thyroid cancer. *Cell Death Dis*. 2018;9(10):1030. doi:10.1038/s41419-018-1054-3
27. Zhao L, Yu Q, Gao C, et al. Studies of the efficacy of low-dose apatinib monotherapy as third-line treatment in patients with metastatic colorectal cancer and apatinib's novel anticancer effect by inhibiting tumor-derived exosome secretion. *Cancers*. 2022;14(10):2492. doi:10.3390/cancers14102492
28. Chen X, Qiu T, Zhu Y, et al. A single-arm, Phase II study of apatinib in refractory metastatic colorectal cancer. *oncologist*. 2019;24(7):407–883. doi:10.1634/theoncologist.2019-0164
29. Rong X, Liu H, Yu H, Zhao J, Wang J, Wang Y. Efficacy of apatinib combined with folfiri in the first-line treatment of patients with metastatic colorectal cancer. *Invest New Drugs*. 2022;40(2):340–348. doi:10.1007/s10637-021-01205-3
30. Chen R, Yang L, Hu S, et al. Apatinib plus 5-fluorouracil as a third or subsequent-line treatment option for metastatic colorectal cancer: a phase-ii, single-arm, prospective study. *Ann Transl Med*. 2022;10(2):100. doi:10.21037/atm-22-77
31. Yu J, Xiao B, Li D, et al. Neoadjuvant camrelizumab plus apatinib for locally advanced microsatellite instability-high or mismatch repair-deficient colorectal cancer (neocap): a single-arm, open-label, Phase 2 study. *Lancet Oncol*. 2024;25(7):843–852. doi:10.1016/S1470-2045(24)00203-1
32. Soumoy L, Ghanem GE, Saussez S, Journe F. Bufalin for an innovative therapeutic approach against cancer. *Pharmacol Res*. 2022;184:106442. doi:10.1016/j.phrs.2022.106442
33. Zou Y, Wang S, Zhang H, et al. The triangular relationship between traditional Chinese medicines, intestinal flora, and colorectal cancer. *Med Res Rev*. 2024;44(2):539–567. doi:10.1002/med.21989
34. Zhang D, Zhai B, Sun J, Cheng J, Zhang X, Guo D. Advances on delivery system of active ingredients of dried toad skin and toad venom. *Int J Nanomed*. 2024;19:7273–7305. doi:10.2147/IJN.S469742
35. Fang K, Zhan Y, Zhu R, et al. Bufalin suppresses tumour microenvironment-mediated angiogenesis by inhibiting the stat3 signalling pathway. *J Transl Med*. 2021;19(1):383. doi:10.1186/s12967-021-03058-z
36. Sheng X, Zhu P, Zhao Y, et al. Effect of pi3k/akt/mtor signaling pathway on regulating and controlling the anti-invasion and metastasis of hepatoma cells by bufalin. *Recent Pat Anticancer Drug Discov*. 2021;16(1):54–65. doi:10.2174/1574892816666210201120324
37. Ding J, Chen X, Gao Z, et al. Metabolism and pharmacokinetics of novel selective vascular endothelial growth factor receptor-2 inhibitor apatinib in humans. *Drug Metab Dispos*. 2013;41(6):1195–1210. doi:10.1124/dmd.112.050310
38. Wang Z, Zhai B, Sun J, et al. Recent advances of injectable in situ-forming hydrogels for preventing postoperative tumor recurrence. *Drug Deliv*. 2024;31(1):2400476. doi:10.1080/10717544.2024.2400476
39. Jia YP, Shi K, Yang F, et al. Multifunctional nanoparticle loaded injectable thermoresponsive hydrogel as nir controlled release platform for local photothermal immunotherapy to prevent breast cancer postoperative recurrence and metastases. *Adv Funct Mater*. 2020;30(25):2001059. doi:10.1002/adfm.202001059
40. Wang Y, Zhang X, Zhang Y, et al. Sprayed hyaluronic acid based multidrug composite hydrogel for postoperative colorectal cancer ultra-efficient long-lasting multi-stage immuno-chemo synergistic therapy. *Mater Horiz*. 2025. doi:10.1039/d5mh00108k
41. Ni Y, Zhao W, Cheng W, et al. Lipopeptide liposomes-loaded hydrogel for multistage transdermal chemotherapy of melanoma. *J Control Release*. 2022;351:245–254. doi:10.1016/j.jconrel.2022.09.014
42. Elkhoury K, Sanchez-Gonzalez L, Lavrador P, et al. Gelatin methacryloyl (gelma) nanocomposite hydrogels embedding bioactive naringin liposomes. *Polymers*. 2020;12(12):2944. doi:10.3390/polym12122944
43. Bi H, Xue J, Jiang H, et al. Current developments in drug delivery with thermosensitive liposomes. *Asian J Pharm Sci*. 2019;14(4):365–379. doi:10.1016/j.ajps.2018.07.006
44. Cui S, Yu L, Ding J. Thermogelling of amphiphilic block copolymers in water: aba type versus ab or bab type. *Macromolecules*. 2019;52(10):3697–3715. doi:10.1021/acs.macromol.9b00534
45. Cao D, Chen X, Cao F, et al. An intelligent transdermal formulation of ala-loaded copolymer thermogel with spontaneous asymmetry by using temperature-induced sol–gel transition and gel–sol (suspension) transition on different sides. *Adv Funct Mater*. 2021;31(22):2100349. doi:10.1002/adfm.202100349
46. Chou T. Drug combination studies and their synergy quantification using the chou-talalay method. *Cancer Res*. 2010;70(2):440–446. doi:10.1158/0008-5472.CAN-09-1947

47. Maswadeh H, Khan A, Alorainy MS, Al-Wabel NA, Demetzos C. In vitro and in vivo activity of thermosensitive liposomes loaded with doxorubicin and cisplatin. *Drug Dev Ind Pharm*. 2022;48(4):158–168. doi:10.1080/03639045.2022.2102648
48. Borys N, Dewhirst MW. Drug development of lyso-thermosensitive liposomal doxorubicin: combining hyperthermia and thermosensitive drug delivery. *Adv Drug Deliv Rev*. 2021;178:113985. doi:10.1016/j.addr.2021.113985
49. Wang P, Chu W, Zhuo X, et al. Modified plga-peg-plga thermosensitive hydrogels with suitable thermosensitivity and properties for use in a drug delivery system. *J Mat Chem B*. 2017;5(8):1551–1565. doi:10.1039/c6tb02158a